

# Spectral Analysis of Input Spike Trains by Spike-Timing-Dependent Plasticity

Matthieu Gilson<sup>1,2\*</sup>, Tomoki Fukai<sup>1</sup>, Anthony N. Burkitt<sup>2,3,4</sup>

**1** Riken Brain Science Institute, Wako-shi, Saitama, Japan, **2** NeuroEngineering Laboratory, Department of Electrical and Electronic Engineering, The University of Melbourne, Melbourne, Victoria, Australia, **3** Centre for Neural Engineering, The University of Melbourne, Melbourne, Victoria, Australia, **4** Bionics Institute, East Melbourne, Victoria, Australia

## Abstract

Spike-timing-dependent plasticity (STDP) has been observed in many brain areas such as sensory cortices, where it is hypothesized to structure synaptic connections between neurons. Previous studies have demonstrated how STDP can capture spiking information at short timescales using specific input configurations, such as coincident spiking, spike patterns and oscillatory spike trains. However, the corresponding computation in the case of arbitrary input signals is still unclear. This paper provides an overarching picture of the algorithm inherent to STDP, tying together many previous results for commonly used models of pairwise STDP. For a single neuron with plastic excitatory synapses, we show how STDP performs a spectral analysis on the temporal cross-correlograms between its afferent spike trains. The postsynaptic responses and STDP learning window determine kernel functions that specify how the neuron “sees” the input correlations. We thus denote this unsupervised learning scheme as ‘kernel spectral component analysis’ (kSCA). In particular, the whole input correlation structure must be considered since all plastic synapses compete with each other. We find that kSCA is enhanced when weight-dependent STDP induces gradual synaptic competition. For a spiking neuron with a “linear” response and pairwise STDP *alone*, we find that kSCA resembles principal component analysis (PCA). However, plain STDP does not isolate correlation sources in general, e.g., when they are mixed among the input spike trains. In other words, it does not perform independent component analysis (ICA). Tuning the neuron to a single correlation source can be achieved when STDP is paired with a homeostatic mechanism that reinforces the competition between synaptic inputs. Our results suggest that neuronal networks equipped with STDP can process signals encoded in the transient spiking activity at the timescales of tens of milliseconds for usual STDP.

**Citation:** Gilson M, Fukai T, Burkitt AN (2012) Spectral Analysis of Input Spike Trains by Spike-Timing-Dependent Plasticity. PLoS Comput Biol 8(7): e1002584. doi:10.1371/journal.pcbi.1002584

**Editor:** Olaf Sporns, Indiana University, United States of America

**Received:** December 1, 2011; **Accepted:** May 14, 2012; **Published:** July 5, 2012

**Copyright:** © 2012 Gilson et al. This is an open-access article distributed under the terms of the Creative Commons Attribution License, which permits unrestricted use, distribution, and reproduction in any medium, provided the original author and source are credited.

**Funding:** Funding is acknowledged from the Australian Research Council (ARC Discovery Project \#DP0771815) and the Japan Science and Technology Agency (Core Research of Evolutional Science and Technology). The Bionics Institute acknowledges the support it receives from the Victorian State Government through the Operational Infrastructure Support Program. The funders had no role in study design, data collection and analysis, decision to publish, or preparation of the manuscript.

**Competing Interests:** The authors have declared that no competing interests exist.

\* E-mail: gilson@brain.riken.jp

## Introduction

Organization in neuronal networks is hypothesized to rely to a large extent on synaptic plasticity based on their spiking activity. The importance of spike timing for synaptic plasticity has been observed in many brain areas for many types of neurons [1,2], which was termed spike-timing-dependent plasticity (STDP). On the modeling side, STDP was initially proposed to capture information within spike trains at short timescales, as can be found in the auditory pathway of barn owls [3]. For more than a decade, STDP has been the subject of many theoretical studies to understand how it can select synapses based on the properties of pre- and postsynaptic spike trains. A number of studies have focused on how STDP can perform input selectivity by favoring input pools with higher firing rates [4,5], with synchronously firing inputs [6], or both [7], detect spike patterns [8] and rate-modulated patterns [9], and interact with oscillatory signals [10,11]. The STDP dynamics can simultaneously generate stability of the output firing rate and competition between individual synaptic weights [6,12–15]. In order to strongly drive the postsynaptic neurons, which we refer to as robust neuronal

specialization. [16]. When considering recurrently connected neurons, the weight dynamics can lead to emerging functional pathways [17–19] and specific spiking activity [20,21]. Recent reviews provide an overview of the richness of STDP-based learning dynamics [22,23].

The present paper aims to provide a general interpretation of the synaptic dynamics at a functional level. In this way, we want to characterize how spiking information is relevant to plasticity. Previous publications [24,25] mentioned the possible relation between STDP and Oja’s rate-based plasticity rule [26], which performs principal component analysis (PCA). Previous work [27] showed how STDP can capture slow time-varying information within spike trains in a PCA-like manner, but this approach does not actually make use of the temporal (approximate) antisymmetry of the typical STDP learning window for excitatory synapses; see also earlier work about storing correlations of neuronal firing rates [28]. Along similar lines, STDP was used to perform independent component analysis (ICA) for specific input signals typically used to discriminate between PCA and ICA [7,29]. In particular, STDP *alone* did not seem capable of performing ICA in those

## Author Summary

Tuning feature extraction of sensory stimuli is an important function for synaptic plasticity models. A widely studied example is the development of orientation preference in the primary visual cortex, which can emerge using moving bars in the visual field. A crucial point is the decomposition of stimuli into basic information tokens, e.g., selecting individual bars even though they are presented in overlapping pairs (vertical and horizontal). Among classical unsupervised learning models, independent component analysis (ICA) is capable of isolating basic tokens, whereas principal component analysis (PCA) cannot. This paper focuses on spike-timing-dependent plasticity (STDP), whose functional implications for neural information processing have been intensively studied both theoretically and experimentally in the last decade. Following recent studies demonstrating that STDP can perform ICA for specific cases, we show how STDP relates to PCA or ICA, and in particular explains the conditions under which it switches between them. Here information at the neuronal level is assumed to be encoded in temporal cross-correlograms of spike trains. We find that a linear spiking neuron equipped with pairwise STDP requires additional mechanisms, such as a homeostatic regulation of its output firing, in order to separate mixed correlation sources and thus perform ICA.

numerical studies: additional mechanisms such as synaptic scaling were necessary. On the other hand, additive-like STDP has been shown to be capable of selecting only one among two identical input pools with independent correlations from each other, also referred to as ‘symmetry breaking’ [13,17]. In addition to studies of the synaptic dynamics, considerations on memory and synaptic management (e.g., how potentiated weights are maintained) have been used to relate STDP and optimality in unsupervised learning [30,31]. To complement these efforts, the present paper proposes an in-depth study of the learning dynamics and examines under which conditions pairwise STDP can perform ICA. For this purpose, we consider input spiking activity that mixes correlation sources. We draw on our previously developed framework that describes the weight dynamics [15,23] and extend the analysis to the case of an *arbitrary* input correlation structure. This theory is based on the Poisson neuron model [6] and focuses on pairwise weight-dependent STDP for excitatory synapses. Mutual information is used to evaluate how STDP modifies the neuronal response to correlated inputs [32]. This allows us to relate the outcome of STDP to either PCA and ICA [33]. Finally, we examine the influence of the STDP and neuronal parameters on the learning process. Our model captures fundamental properties shared by more elaborate neuronal and STDP models. In this way, it provides a minimal and tractable configuration to study the computational power of STDP, bridging the gap between physiological modeling and machine learning.

## Results

Spectral decomposition is typically used to find the meaningful components or main trends in a collection of input signals (or data). In this way, one can represent or describe the inputs in a summarized manner, i.e., in a space of lower dimension. This paper focuses on the information conveyed by spike trains, which will be formalized later. The function of neuronal processing is to extract the dominant component(s) of the information that it receives, and disregard the rest, such as noise. In the context of

learning, synaptic competition favors some weights at the expense of others, which tunes the neuronal selectivity. As a first step to introduce spectral decomposition, we consider Oja’s rule [26] that enables a linear non-spiking neuron to learn the correlations between its input firing rates. At each time step, the 100 input firing rates are determined by two Gaussian profiles with distinct means, variances and amplitudes (green and blue curves in Fig. 1D), in addition to noise. The area under the curve indicates the strength of input correlations; here the green dashed curve “dominates” the blue dashed-dotted curve. This results in correlation among the input rates, as represented by the matrix in Fig. 1A. The vector of weights  $\mathbf{w}$  is modified by Oja’s rule:

$$\dot{\mathbf{w}} \propto y * (\mathbf{x} - y * \mathbf{w}), \quad (1)$$

where  $\mathbf{x}$  is the input rates and  $y = \mathbf{x} \bullet \mathbf{w}$  is the neuron output ( $\bullet$  indicates the scalar product of the two vectors). The weight evolution is represented in Fig. 1B. The final weight distribution reflects the principal component of the correlation matrix (red solid curve in Fig. 1C). As shown in Fig. 1D, this does not represent only the stronger correlation source (green dashed curve), but also the weaker one (blue dashed-dotted curve). This follows because the principal component mixes the two sources, which overlap in Fig. 1A. In other words, Oja’s rule cannot isolate the strongest source and thus cannot perform ICA, but only PCA. We will examine later whether the same phenomenon occurs for STDP. Note that the rate correlation matrix is always symmetric. This differs from using PCA in the context of data analysis, such as finding the direction that provides the dependence of highest magnitude in a cloud of data points.

## Spiking neuron configuration

In order to examine the computational capabilities of STDP, we consider a single neuron whose  $N$  excitatory synapses are modified by STDP, as shown in Fig. 2A. Our theory relies on the Poisson neuron model, which fires spikes depending on a stochastic rate intensity that relates to the soma potential. Each presynaptic spike induces variation of the soma potential, or postsynaptic potential (PSP), described by the normalized kernel function  $\epsilon_i$ , shifted by the axonal and dendritic delays,  $d_i^{\text{den}}$  and  $d_i^{\text{ax}}$ , respectively (Fig. 2B). The size of the PSP is scaled by the synaptic weight  $w_i$ .

**Pairwise weight-dependent STDP model.** We use a phenomenological STDP model described by a learning window  $W(w_i; \Delta t)$  as in Fig. 2C. Importantly, LTP/LTD is not determined by the relative timing of firing at the neuron somas, but by the time difference at the synaptic site, meaning that  $\Delta t$  incorporates the axonal and dendritic delays. This choice can be related to more elaborate plasticity models based on the local postsynaptic voltage on the dendrite [7,34].

We will examine common trends and particularities of the weight specialization for several models of STDP.

- A “plain” STDP model postulates that all pairs of pre- and postsynaptic spikes, and only them, contribute to the weight modification, provided the time difference  $\Delta t$  is in the range of the learning window  $W$  as illustrated in Fig. 2D.
- A second scheme assumes that, in addition to STDP-specific weight updates, each pre- or postsynaptic spike also induces a weight update via the corresponding contribution  $a^{\text{in/out}}$ , as illustrated in Fig. 2D. This will be referred to as ‘STDP+SSC’, as opposed to ‘plain STDP’ (or ‘STDP’ alone when no precision is needed). Although sometimes regarded as less plausible from a biological point of view, single-spike

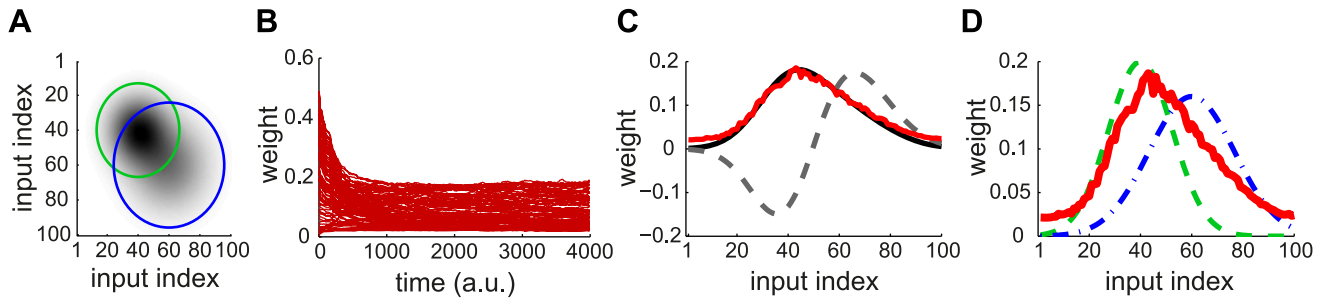


**Figure 1. Example of PCA performed by Oja's rate-based plasticity rule.** (A) Theoretical cross-correlation matrix of 100 inputs induced by two Gaussian distributions of rates. Darker pixels indicate higher correlations. The circles indicate where the correlation for each source drops below 10% of its maximum (see the Gaussian profiles in D). (B) Traces of the weights modified by Oja's rule [26] in (1). At random times, the input rates  $x$  follow either Gaussian rate profile corresponding to the green and blue curves in D; white noise is added at each timestep. (C) The asymptotic distribution of the weights (red) is close to the principal component of the matrix in A (black solid curve), but distinct from the second component (black dashed curve). (D) The final weight distribution (red) actually overlaps both Gaussian rate profiles in green dashed and blue dashed-dotted lines that induce correlation in the inputs. The green and blue curves correspond to the small and large circles in A, respectively.  
doi:10.1371/journal.pcbi.1002584.g001

contributions can regulate the neuronal output firing in a homeostatic fashion [35,36]. In particular, we will examine the role of  $a^{\text{out}} < 0$  that has been used to enhance the competition between synaptic inputs [6].

- We will consider weight dependence for STDP, namely how the learning window  $W(w_i; \Delta t)$  depends on the weight  $w_i$  as in Fig. 2C, following experimental observations

[37]. Figure 2E represents four examples of weight dependence: our 'log-STDP' in blue [16], the weight-independent 'add-STDP' for additive STDP [6,12], 'nlta-STDP' proposed by Güting et al. [13], and 'mlt-STDP' for the multiplicative STDP by van Rossum et al. [38] in which LTD scales linearly with  $w_i$ . For log-STDP and nlta-STDP, the weight dependence can be adjusted via a parameter. For log-STDP (left panel), the

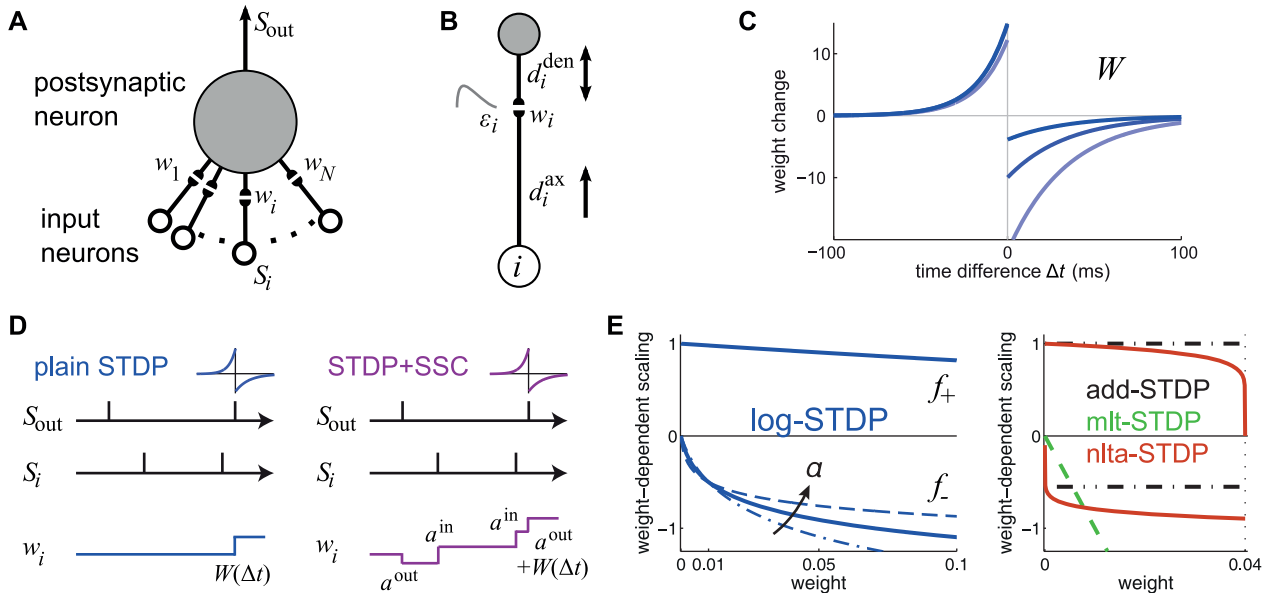


**Figure 2. Single neuron with STDP-plastic excitatory synapses.** (A) Schematic representation of the neuron (top gray-filled circle) and the  $N$  synapses (pairs of black-filled semicircles) that are stimulated by the input spike trains  $S_i$  (bottom arrows). (B) Detail of synapse  $i$ , whose weight is  $w_i$ , postsynaptic response kernel  $\epsilon_i$ , axonal and dendritic delays  $d_i^{\text{den}}$  and  $d_i^{\text{ax}}$ , respectively. The arrows indicate that  $d_i^{\text{ax}}$  describes the propagation along the axon to the synapse, while  $d_i^{\text{den}}$  relates to both conduction of postsynaptic potential (PSP) toward soma and back-propagation of action potential toward the synaptic site. (C) Example of temporally Hebbian weight-dependent learning window  $W(w_i; \Delta t)$  that determines the STDP contribution of pairs of pre- and postsynaptic spikes. The curve corresponds to (22). Darker blue indicates a stronger value for  $w_i$ , which leads to less potentiation and more depression. (D) Schematic evolution of the weight  $w_i$  for given pre- and postsynaptic spike trains  $S_i$  and  $S_{\text{out}}$ . The size of each jump is indicated by the nearby expression. Comparison between plain STDP for which only pairs contribute and STDP+SSC where single spikes also modify the weight via the terms  $a^{\text{in/out}}$ . Here only the pair of latest spikes falls into the temporal range of STDP and thus significantly contributes to STDP. (E) Scaling functions of  $f_{\pm}$  that determine the weight dependence for LTP and LTD. In the left panel, the blue solid curve corresponds to log-STDP [16] with  $w_0 = 0.01$ ,  $\alpha = 5$  and  $\beta = 50$  in (23). The parameter  $\alpha$  controls the saturation of the LTD curve: the dashed curve corresponds to  $\alpha = 20$  and the dashed-dotted curve to  $\alpha = 1$ . In the right panel, the red solid curves represent  $f_{\pm}$  for nlta-STDP [13] with  $\gamma = 0.1$  and  $w_{\text{max}} = 0.04$  in (24); the black dashed-dotted horizontal lines indicate the add-STDP that is weight independent; the green dashed line corresponds to a linearly dependent LTD for mlt-STDP [38].  
doi:10.1371/journal.pcbi.1002584.g002

LTD curve scales almost linearly with respect to  $w_i$  for small values of  $\alpha > 0$  in a similar manner to mlt-STDP, whereas it is additive-like (weight-independent) STDP for large values of  $\alpha$  (in the range  $w_i \geq w_0$ ). Likewise, nlta-STDP scales between the other ‘multiplicative’ STDP proposed by Rubin et al. [39] for  $\gamma = 1$  and add-STDP for  $\gamma = 0$ ; the red curve in Fig. 2E uses  $\gamma = 0.1$ .

Variability is also incorporated in the weight updates through the white noise  $\eta$ , although its effect will not be examined specifically in the present work. Typical parameters used in simulations are given in Table 1 and detailed expressions for  $W$  are provided in Methods.

**Learning dynamics.** The present analysis is valid for any pairwise STDP model that is sensitive to up-to-second order spike-time correlations. In its present form, it cannot deal with, for example, the ‘triplet’ STDP model [40] and the stochastic model proposed by Appleby and Elliott [41]. The neuronal spiking activity is described by the corresponding firing rates and spike-time correlations. See Table 2 for an overview of the variables in our system. The input rates and correlations are assumed to be consistent over the learning epoch. Details of the analytical calculations are provided in Methods. The evolution of the vector of plastic weights  $\mathbf{w}$  is then governed by the following differential equation:

$$\dot{\mathbf{w}} \propto Y(\mathbf{w}; \mathbf{v}_{\text{in}}; \mathbf{v}_{\text{out}}) + \mathbf{w} \mathbb{C}^Z(\mathbf{w}), \quad (2)$$

where the dependence over time  $t$  is omitted. The function  $Y$  lumps rate contributions to plasticity (including STDP) and depends on the vector of input firing rates  $\mathbf{v}_{\text{in}}$  and neuronal output firing rate  $\mathbf{v}_{\text{out}}$ , as well as the weights. The second term describes STDP-specific spike-based effects. The STDP effect are described by the matrix  $\mathbb{C}^Z(\mathbf{w}) = \mathbb{C}^Z(\mathbf{w}, t)$ , which is assumed to be independent of  $t$  and whose elements are:

$$\mathbb{C}_{ij}^Z(\mathbf{w}; t) = \int_{-\infty}^{+\infty} \chi_i(w_j; \tau) C_{ij}(t, \tau) d\tau, \quad (3)$$

namely the (anti)convolution of the input spike-time cross-correlograms  $C_{ij}(\tau)$  with the kernel functions  $\chi_i(w_j; \tau)$ , for each pair of inputs  $i$  and  $j$ . A schematic example is illustrated in Fig. 3A. For clarity purpose, we rewrite the time difference  $\Delta t$  as  $\tau$  hereafter. In (3), each kernel  $\chi_i$  combines the STDP learning window at synapse  $j$  and the postsynaptic response kernels  $\epsilon_i$ :

$$\chi_i(w_j; \tau) := [W(w_j; \cdot) * \epsilon_i(\cdot)](\tau - 2d_i^{\text{den}}), \quad (4)$$

where the convolution indicated by  $*$  concerns the variable  $\tau$ , as illustrated in Fig. 3B. For weight-dependent STDP, the kernel is modified via the scaling of both potentiation and depression for  $W(w_j; \cdot)$  in terms of  $w_j$  (Fig. 2C). In addition, the postsynaptic response crucially shapes  $\chi_i$  [19,27], as shown in Fig. 3C. In the case of a single neuron (as opposed to a recurrent network), the dendritic delay  $d_i^{\text{den}}$  plays a distinct role compared to the axonal delay  $d_i^{\text{ax}}$  in that it shifts the kernel  $\chi_i$  as a function of  $\tau$  to the right, namely implying more potentiation for  $\tau = 0$ .

## Encoding the input correlation structure into the weight structure

We stress that the novel contribution of the present work lies in considering general input structures, i.e., when the matrix of cross-correlograms  $\mathbb{C}(\tau)$  is arbitrary. This extends our previous study

**Table 1.** Neuronal and learning parameters.

Quantity:	variable name and value
time step	$10^{-4}$ s
simulation duration	500 s
<b>Input parameters</b>	
input firing rate	$v_0 = 10$ sp/s
input correlation strength	$c \leq 0.4$
<b>PSP parameters</b>	
synaptic rise time constant	$\tau_A = 1$ ms
synaptic decay time constant	$\tau_B = 5$ ms
axonal delays	$d_i^{\text{ax}} = 4 \pm 1$ ms
dendritic delays	$d_i^{\text{den}} = 0$ ms
<b>STDP model</b>	
learning speed	$\eta = 2 \times 10^{-4}$
LTP time constant	$\tau_+ = 17$ ms
LTD time constant	$\tau_- = 34$ ms
white noise standard deviation	$\sigma = 0.6$
<b>log-STDP in (23)</b>	
LTP scaling coefficient	$A_+ = 1$
LTP decay factor	$\beta = 50$
LTD scaling coefficient	$A_- = 0.5$
LTD curvature factor	$\alpha = 5$
reference weight	$w_0 = 0.005$
<b>nlta-STDP in (24)</b>	
LTP scaling coefficient	$A_+ = 1$
LTD scaling coefficient	$A_- = 0.8$
weight-dependence exponent	$\gamma = 0.1$
weight upper bound	$w_{\text{max}} = 0.04$
<b>add-STDP</b>	
LTP scaling coefficient	$A_+ = 1$
LTD scaling coefficient	$A_- = 0.55$
weight upper bound	$w_{\text{max}} = 0.04$
<b>mlt-STDP in (25)</b>	
LTP scaling coefficient	$A_+ = 1$
LTD scaling coefficient	$A_- = 100$
<b>single-spike plasticity terms (SCC)</b>	
presynaptic contribution	$a^{\text{in}} = 0.1$
postsynaptic contribution	$a^{\text{out}} = -0.05$

Unless specified, the above parameters are used in numerical simulation.  
doi:10.1371/journal.pcbi.1002584.t001

[15] of the case of homogeneous within-pool correlations and no between-pool correlations, the matrix  $\mathbb{C}^Z$  in (3) is diagonal (by block). We focus on the situation where the average firing rates across inputs do not vary significantly. This means that rate-based plasticity rules cannot extract the spiking information conveyed by these spike trains. In this case, pairwise spike-time correlations mainly determine the weight specialization induced by STDP via  $\mathbf{w} \mathbb{C}^Z(\mathbf{w})$ , dominating rate effects lumped by  $Y$  in (2). The key is the spectral properties of  $\mathbb{C}^Z$ , which will be analyzed as follows:

- evaluation of the equilibrium value for the mean weight  $w_{\text{av}}^*$  in the uncorrelated case;

**Table 2.** Variables and parameters that describe the neuronal learning system.

Description	symbol	(vector/matrix notation)
input firing rates	$v_i(t)$	$\mathbf{v}_{in}(t)$
input spike-time cross-covariances	$C_{ij}(t, \tau)$	$\mathbb{C}(t, \tau)$
neuronal firing rate	$v_{out}(t)$	
input-output spike-time covariances	$F_i(t, \tau)$	$\mathbf{F}(t, \tau)$
synaptic weights	$w_i(t)$	$\mathbf{w}(t)$
PSP function	$c_i(t)$	
axonal delays	$d_i^{ax}$	
dendritic delays	$d_i^{den}$	
kernel functions for synapse $j$	$\chi_j(w_j, \tau)$	
lumped plasticity rate-based effects		$Y(\mathbf{w}; \mathbf{v}_{in}; v_{out})$
STDP-specific plasticity spike effects	$C'_{ij}(\mathbf{w}; t)$	$\mathbb{C}'(\mathbf{w}; t)$
integral value of STDP	$\tilde{W}(w)$	

The variable  $t$  denotes the time, whereas  $\tau$  indicates the spike-time difference (or time lag) used in correlations and covariances.  
doi:10.1371/journal.pcbi.1002584.t002

- calculation of the matrix  $\mathbb{C}'(\mathbf{w}^*)$  that combines the input correlation structure, the PSP and STDP parameters ( $\mathbf{w}^*$  is the homogeneous weight vector for which  $w_i = w_{av}^*$  for all  $i$ );
- analysis of the spectrum of  $\mathbb{C}'(\mathbf{w}^*)$  to find the dominant eigenvalue(s) and the corresponding left-eigenvector(s);
- decomposition of the initial weight structure (e.g., homogeneous distribution) in the eigenspace to predict the specialization.

**Equilibrium for the mean weight  $w_{av}^*$ .** Partial stability of the synaptic dynamics is necessary in order that not all weights cluster at zero or tend to continuously grow. This also implies the stabilization of the output firing rate. Here we require that the STDP dynamics itself provides a stable fixed point for  $w_{av}^*$ . In particular, this must be true for uncorrelated inputs, which relates to equating to zero the term  $Y(\mathbf{w}; \mathbf{v}_{in}; v_{out})$  in (2).

For plain STDP with weight dependence, the corresponding fixed point is determined by the STDP learning window alone, which is the same for all weights  $w_i$  here and is related to the integral value

$$\tilde{w}(w_i^*) = 0. \quad (5)$$

Here the weight dependence alone can stabilize the mean synaptic weights, which requires that  $\tilde{w}(w)$  decreases when  $w$  increases [13,38,42].

For STDP+SCC, a mean-field approximation of  $Y(\mathbf{w}; \mathbf{v}_{in}; v_{out})$  over the pool of incoming synapses is often used to evaluate the stability of the mean weight  $w_{av} = \sum_i w_i / N$ , which gives  $a^{in} v_0 + a^{out} v_{out} + \tilde{w}(w_{av}) v_0 v_{out} \simeq 0$ , where  $v_0 = \sum_i v_i / N$  is the mean input firing rate. The equilibrium values for the mean weight  $w_{av}^*$  and the neuronal firing rate  $v_{out}^*$  are then related by

$$v_{out}^* \simeq - \frac{a^{in} v_0}{a^{out} + \tilde{w}(w_{av}^*) v_0}. \quad (6)$$

A stable fixed point for arbitrary input configuration is ensured by  $a^{in} > 0$ ,  $a^{out} < 0$  and a negative derivative  $\tilde{w}'(w) \leq 0$  as a function of  $w$  as well as  $\tilde{w}(w_{av}^*) < 0$  at the weight equilibrium value [19]. This means that the right-hand side is a negative function of  $w_{av}^*$ . Note that the additional condition  $a^{in} + a^{out} > 0$  is required for networks with plastic recurrent synapses [43]. The plasticity terms  $a^{in/out}$  can lead to a homeostatic constraint on the output firing rate  $v_{out}$  [35]. In the case of stability, the equilibrium values  $v_{out}^*$  and  $w_{av}^*$  depend on the respective input firing rate  $v_i$ . For weight-dependent STDP+SCC, fixed points  $w_i^*$  also exist for individual weights  $w_i$  and correspond to (6) when replacing  $v_0$  by  $v_i$  and  $w_{av}$  by  $w_i^*$ . The implications of these two different ways of stabilizing  $w_{av}$  will be discussed via numerical results later.

**Spectrum of  $\mathbb{C}'(\mathbf{w}^*)$  and initial weight specialization.** Following our previous study [16], we consider that rate-based effects vanish and focus on the initial stage when weights specialize due to the spike-time correlation term involving  $\mathbb{C}'$  in (2). This means that we approximate

$$\dot{\mathbf{w}} \simeq \eta \mathbf{w} \mathbb{C}'(\mathbf{w}^*). \quad (7)$$

The weight evolution can be evaluated using (7) provided spike-time correlations are significantly strong compared to the “noise” in the learning dynamics. The rate terms in  $Y$  are proportional to the  $v_0 v_{out}$  whereas the spike-based term grow with  $v_0$  only. This implies stronger noise and more difficulty to potentiate weights when  $v_{out}$  is high at the baseline state, e.g., for large input firing rates. Assuming homogeneous weights  $w_i \simeq w_{av}^*$  as initial condition, the weight dynamics is determined by the learning window  $W(w_i; \cdot) \simeq W(w_{av}^*; \cdot)$ . As a first step, we consider the case where the matrix  $\mathbb{C}'(\mathbf{w}^*)$  is diagonalizable as a real matrix, namely  $\mathbb{C}' = \mathbb{P}^{-1} \mathbb{D} \mathbb{P}$  with  $\mathbb{D}$  a diagonal matrix and  $\mathbb{P}$  the matrix for the change of basis (all with real elements). The rows of  $\mathbb{P}$  are the orthogonal left-eigenvectors  $\tilde{\mathbf{v}}_l$  corresponding to the eigenvalues  $\lambda_l$ ,  $0 \leq l \leq N$  that are the diagonal elements of  $\mathbb{D}$ . The weight vector  $\mathbf{w}$  can be decomposed in the basis of eigenvectors (or spectral components)

$$\mathbf{w}(t) = \sum_l \alpha_l(t) \tilde{\mathbf{v}}_l, \quad (8)$$

where  $\alpha_l$  are the coordinates of  $\mathbf{w}$  in the new basis. By convention, we require all  $\tilde{\mathbf{v}}_l$  to be normalized and that  $\alpha_l(0) > 0$  at time  $t=0$  for  $\mathbf{w} = \mathbf{w}^*$ . Transposing (7) in the new basis, the evolution of  $\alpha_l$  can be approximated by  $\dot{\alpha}_l \simeq \eta \lambda_l \alpha_l$ , which gives

$$\mathbf{w} \simeq \eta \sum_l \alpha_l(0) \exp(\lambda_l t) \tilde{\mathbf{v}}_l. \quad (9)$$

The initial weight specialization is thus dominated by the  $\alpha_l$  related to the largest positive eigenvalues  $\lambda_l$  and can be predicted by the corresponding eigenvectors  $\tilde{\mathbf{v}}_l$  [19,25].

In general, we can use the property that the set of diagonalizable matrices with complex elements is dense in the vector space of square matrices [44, p 87]. This means that it is possible to approximate  $\mathbb{C}'(\mathbf{w}^*) \simeq \mathbb{P}^{-1} \mathbb{D} \mathbb{P}$ , in which case  $\mathbb{D}$  and  $\mathbb{P}$  may have non-real elements. If the eigenvalue with the largest real part is a real number, the same conclusion as above is expected to hold,

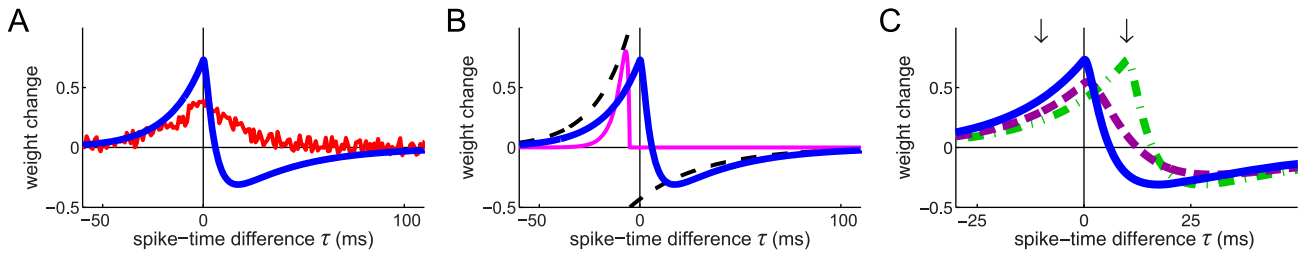


**Figure 3. Kernel function  $\chi$ .** (A) Anticonvolution of a fictive correlogram  $C_{ij}(\tau)$  (red curve) and a typical kernel function  $\chi_i(\cdot, \tau)$  (blue curve). The amount of LTP/LTD corresponds to the area under the curve of the product of the two functions. (B) Plot of a typical kernel  $\chi_i(w_0, \tau)$  as a function of  $\tau$  (blue curve). It corresponds to (4) for log-STDP with the baseline parameters in Table 1, namely rise and decay time constants  $\tau_A = 1$  and  $\tau_B = 5$  ms in (29), respectively, and a purely axonal delay  $d_i^{\text{ax}} = 5$  ms. The related STDP learning window  $W(w_0; \tau)$  is plotted in black dashed line and the mirrored PSP response in pink solid line. The effect of the axonal delay shifts both the  $W$  and the PSP in the same direction, which cancels out. (C) Variants of  $\chi_i(w_0, \tau)$  for longer PSP time constants,  $\tau_A = 2$  and  $\tau_B = 10$  ms (purple curve); and for a dendritic delay  $d_i^{\text{den}} = 5$  ms (green dashed-dotted curve). In contrast to  $d_i^{\text{ax}}$  that does not play a role in (4),  $d_i^{\text{den}}$  shifts  $\chi_i$  to the right. The arrows indicate  $\tau = \pm 10$  ms. doi:10.1371/journal.pcbi.1002584.g003

even though the eigenvectors may not be orthogonal. When a pair of eigenvalues dominate the spectrum,  $\lambda_1$  and its conjugate  $\lambda_1^*$ . The decomposition of the homogeneous vector  $\mathbf{w}^*$  on the plane of the corresponding eigenvectors that gives  $2\Re\{\alpha_1(0)\tilde{\mathbf{v}}_1\lambda_1\}$  leads to the dominant term  $2\Re\{\alpha_1(0)\tilde{\mathbf{v}}_1 \exp(\lambda_1 t)\}$  in the equivalent to (9);  $\Re$  denotes the real part here. The initial growth or decay of  $w_i$  is given by the derivative:

$$\dot{\mathbf{w}} \simeq \eta \Re\{\alpha_1(0)\tilde{\mathbf{v}}_1\lambda_1\} = \eta \mathbf{v}_1. \quad (10)$$

Note that this expression applies to the real case too, where  $\mathbf{v}_1 \propto \tilde{\mathbf{v}}_1$  and the convention  $\alpha_1(0) > 0$  simply means that  $\tilde{\mathbf{v}}_1$  reflects the signs of the elements of the derivative vector.

In most cases, the spectrum is dominated as described above and we can use the expression (10), which will be referred to as the ‘strongest’ spectral component of  $\mathcal{C}^Z(\mathbf{w})$ . Note that, in the case of a non diagonalizable matrix, the Jordan form of  $\mathcal{C}^Z(\mathbf{w})$  could be used to describe more precisely the weight evolution, for example. We have also neglected the case  $\alpha_1 \simeq 0$  for  $\mathbf{w}^*$ , for which the decomposition of the before-learning weight specialization  $\mathbf{w}(t=0)$  may also play a role. Nevertheless, noise in the weight dynamics will lead the system away from such unstable fixed points.

**Asymptotic weight structure and stability.** Now we focus on the final weight distribution that emerges, following the initial splitting. In particular, a stable asymptotic structure can be obtained when the learning equation (2) has a (stable) fixed point, as illustrated in Fig. 4A for the simple case of two weights  $w_1$  and  $w_2$ . Weight dependence can lead to the existence of at least a realizable and stable fixed point. Two conditions ensure the existence of a solution to the learning equation. First, the weight dependence should be such that LTD vanishes for small weights while LTP vanishes for large weights, as is the case for both log-STDP and nlta-STDP for  $\gamma > 0$ . Second, the inputs should be positively correlated. If this second assumption is lifted, the fixed point may become unrealizable (e.g.,  $w_i^* < 0$ ) or simply not exist as in Fig. 4B. Nevertheless, we can also conclude the existence of a stable fixed point in the range of *small* negative correlations. This follows because of the continuity of the matrix coefficients in (2), which determines the fixed points  $w_i^*$ , with respect to the matrix elements of  $\mathcal{C}^Z$ .

A general result about the relationship between the fixed point(s) and  $\mathcal{C}^Z(\mathbf{w}^*)$  is a difficult problem because  $\mathcal{C}^Z(\mathbf{w})$  changes together with  $\mathbf{w}$  for a weight-dependent learning window  $W$ . This implies

that the eigenvector basis  $\{\mathbf{v}_i\}$  are modified together with  $\mathbf{w}$ . With the further assumption of a weak weight dependence and for a single dominant eigenvector  $\mathbf{v}_1$ , the term  $\mathbf{w}\mathcal{C}^Z(\mathbf{w})$ , which determines the weight specialization, remains similar to  $\mathbf{v}_1$ . By this, we mean that the elements of both vectors are sorted in the same order. At the equilibrium, rate-based effects lumped in  $Y$  balance the spike-based effects that are qualitatively described by  $\mathbf{v}_1$ . Under our assumptions, the vector elements of  $Y$  are decreasing functions of the weights  $w_j$ . It follows that inputs corresponding to larger elements of (10) end up at a higher level of potentiation. However, when  $\mathcal{C}^Z$  has a strong antisymmetric component due to negative matrix elements, it can exhibit complex conjugate dominant eigenvalues with large imaginary parts. The weight vector  $\mathbf{w}$  may experience a rotation-like evolution, in which case the final distribution differs qualitatively from the initial splitting. Nevertheless, the weights with strongest initial LTP are expected to be mostly potentiated eventually. Further details are provided in Methods. Deviation from the predictions can also occur when several eigenvalues with similar real parts dominate the spectrum.

In the particular case of *additive* STDP, a specific issue arises since the existence of a fixed point is not guaranteed. When  $\mathcal{C}^Z(\cdot)$

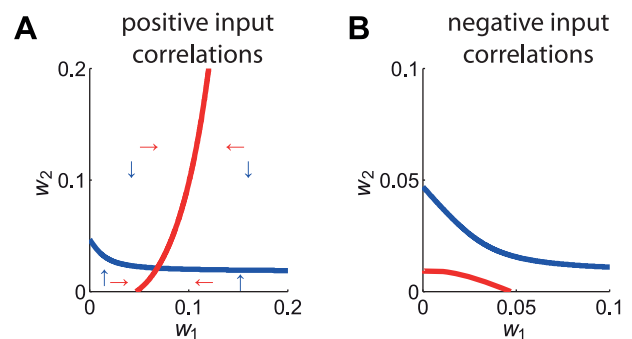


**Figure 4. Existence of a fixed point for the weight dynamics.** (A) Curves of the zeros of (39) for  $N=2$  weights in the case of positively correlated inputs. The two curves have an intersection point, as the equilibrium curve for  $w_1$  in red spans all  $w_2 \in [0, 0.2]$ , while that for  $w_2$  in blue spans all  $w_1 \in [0, 0.2]$ . The arrows indicate the signs of the derivatives  $\dot{w}_1$  and  $\dot{w}_2$  in each quadrant (red and blue, resp.). (B) Similar to A with negative input correlations, for which the curves do not intersect. doi:10.1371/journal.pcbi.1002584.g004

has purely complex eigenvalues, the weight dynamics are expected to exhibit an oscillatory behavior that may impair the emergence of an asymptotic weight structure, as was pointed out by Sprekeler et al. [27]. An example with add-STDP+SCC and eigenvalues that have large imaginary parts is provided in Text S1.

As some weights grow larger, they compete to drive the neuronal output firing [12]. This phenomenon is relatively weak for Poisson neurons compared to integrate-and-fire neurons [16]. For STDP+SCC, synaptic competition is enhanced when using  $a^{\text{out}} < 0$ . Following (6), the larger negative  $a^{\text{out}}$  is, the lower the output firing rate  $v_{\text{out}}$  that is maintained by STDP at the equilibrium. This also holds when inputs are correlated. These rate effects lead to a form of sparse coding in which fewer weights are significantly potentiated, while the remainder weights are kept small. Another interpretation of the effect of  $a^{\text{out}}$  relies on the fact that all weights are homogeneously depressed after postsynaptic spiking. Then, only the weights of inputs involved in triggering firing may not experience depression provided STDP sufficiently potentiate them. This concerns inputs related to a common correlation source and may result in a winner-take-all situation. Moreover, this effect increases with the output firing rate and may become dominant when STDP generates strong LTP, leading to large weights.

In summary, for plain STDP, the final weight structure for plain STDP is expected to reflect the initial splitting, which is determined by the strong spectral component of  $\mathbb{C}^Z(\mathbf{w}^*)$  in (10), at least for the most potentiated weights that win the competition. The assumption of “sufficiently weak” weight dependence holds for log-STDP with  $\alpha \gg 1$  (sublinear saturation for  $w_i \geq w_0$ ) and for nlt-STDP with small values of  $0 < \gamma \leq 0.1$  (for  $w_i$  away from the bounds). STDP+SCC may modify the final weight distribution when the single-spike contributions have comparably strong effects to STDP. In particular, competition between correlation sources is expected to be enhanced when  $a^{\text{out}}$  is sufficiently large negative. In the following sections, we verify these predictions using numerical simulation for various input configurations.

### Input spike-time correlation structure

In order to illustrate the above analysis, we consider input configurations that give to “rich” matrices of pairwise correlations  $\mathbb{C}$ . Model input spike trains commonly combine stereotypical activity and random “background” spikes. Namely, to predict the evolution of plastic synaptic weights, it is convenient that the statistical properties of the inputs are invariant throughout the learning epoch (e.g., the presentation of a single stimulus). Mathematically, we require the input spike trains to be second-order stationary. In this way, the input firing rates  $\mathbf{v}_{\text{in}} = \mathbf{v}_{\text{in}}(t)$  and the spike-time correlograms  $\mathbb{C}(\tau) = \mathbb{C}(t, \tau)$  in (2) are well-defined and practically independent of time  $t$ , even though the spike trains themselves may depend on time. The formal definitions of  $\mathbf{v}_{\text{in}}$  and  $\mathbb{C}(\tau)$  in Methods combine a stochastic ensemble average and a temporal average. This allows to deal with a broad class of inputs that have been used to investigate the effect of STDP, such as spike coordination [6,13,14,36] and time-varying input signals that exhibit rate covariation [12,27,45], as well as elaborate configurations proposed recently [46–48]. Most numerical results in the present paper use the spike coordination that mixes input correlation sources. In the last section of Results, rate covariation will also be examined for the sake of generality.

**Pools with mixed spike-time correlation.** Inputs thus generated model signals that convey information via precise timing embedded in noisy spike trains. A simple example consists of instantaneously correlated spike trains that correspond to input neurons belonging to the same afferent pathway, which have been widely used to study STDP dynamics [13,14,36]. Here we also

consider the situation where synapses can take part in conveying distinct independent signals, as well as time lags between the relative firing of inputs. To do so, spike trains are generated using a thinning of homogeneous Poisson processes. Namely, independent homogeneous Poisson processes are used as references  $\mathcal{R}_k$  to determine correlated events at a given rate  $v_{\mathcal{R}}^k$  that trigger for some designated inputs. For input  $i$ , we denote  $n_i^k \geq 0$  the number of spikes associated with each correlated event from  $\mathcal{R}_k$ . The probability of firing after a given latency  $\mathcal{G}_{i,p}^k$  is  $\sqrt{c_{i,p}^k}$  with  $1 \leq p \leq n_i^k$ . Outside correlated events, inputs randomly fire spikes such that they all have the same time-averaged firing rate  $v_0$ . This corresponds to an additional Poisson process with rate  $v_0 - \sum_{k,p} v_{\mathcal{R}}^k \sqrt{c_{i,p}^k}$ , summing over all independent references indexed by  $k$ . As a result, for two inputs  $i$  and  $j$  related to a single common reference  $\mathcal{R}_k$ , the between-pool cross-covariance is given by

$$C_{ij}(\tau) = \sum_{p,p'} v_{\mathcal{R}}^k \sqrt{c_{i,p}^k c_{j,p'}^k} \delta(\tau - \mathcal{G}_{i,p}^k + \mathcal{G}_{j,p'}^k), \quad (11)$$

where  $\delta$  is the Dirac delta function. The correlogram comprises delta peaks at the time difference between all pairs of spikes (indexed by  $p$  and  $p'$ , respectively) coming from inputs  $i$  and  $j$ . The covariance contributions in (11) from distinct references summate. This method of generating input pattern activity is an alternative to that used in previous studies [8,9], but it produces similar correlograms.

### Extraction of the principal spectral component

This first application shows how STDP can perform PCA, which is the classical spectral analysis for symmetric matrices. To do so, we consider input pools that have multiple sources of correlated activity, which gives within-pool and between-pool correlations. In the example in Fig. 5A, inputs are partitioned into  $m=4$  pools of 50 inputs each that have the same firing rate  $v_0 = 10\text{sp/s}$ . Some pools share common references that trigger coincident firing as described in (11): pools  $\bar{1}$  and  $\bar{2}$  (from left to right) share a correlation reference  $\mathcal{R}_1$  with respective correlation strengths  $\bar{c}_1^1 = 0.4$  and  $\bar{c}_2^1 = 0.1$  for the concerned inputs; pools  $\bar{2}$  and  $\bar{3}$  share  $\mathcal{R}_2$  with  $\bar{c}_2^2 = \bar{c}_3^2 = 0.2$ ; and pools  $\bar{3}$  and  $\bar{4}$  share  $\mathcal{R}_3$  with  $\bar{c}_3^3 = \bar{c}_4^3 = 0.1$ . The overline indicates pool variables. All references  $k$  correspond to coincident firing ( $\mathcal{G}_{i,1}^k = 0$ ) and the rate of correlated events is  $v_{\mathcal{R}}^k = v_0$ . The matrix  $\mathbb{C}(\tau)$  is composed of blocks and given by

$$\bar{\mathbb{C}}(\tau) = \mathbb{Q}^T \mathbb{Q} v_0 \delta(\tau), \quad (12)$$

$$\text{with } \mathbb{Q} = \begin{pmatrix} \sqrt{\bar{c}_1^1} & \sqrt{\bar{c}_1^2} & 0 & 0 \\ 0 & \sqrt{\bar{c}_2^2} & \sqrt{\bar{c}_3^2} & 0 \\ 0 & 0 & \sqrt{\bar{c}_3^3} & \sqrt{\bar{c}_4^3} \end{pmatrix}.$$

Each row of  $\mathbb{Q}$  corresponds to a single correlation source here. We further assume that all synapses have identical kernels  $\chi_i = \chi$ . Combining (11) and (3), their covariance matrix  $\mathbb{C}^Z$  reads

$$\bar{\mathbb{C}}^Z(w_{\text{av}}^*) = \int_{-\infty}^{+\infty} \chi(w_{\text{av}}^*, \tau) \bar{\mathbb{C}}(\tau) d\tau$$

$$= v_0 \chi(w_{\text{av}}^*, 0) \begin{pmatrix} 0.4 & 0.2 & 0 & 0 \\ 0.2 & 0.3 & 0.2 & 0 \\ 0 & 0.2 & 0.3 & 0.1 \\ 0 & 0 & 0.1 & 0.1 \end{pmatrix}. \quad (13)$$

The covariance matrix  $\tilde{C}^Z(w_{av}^*)$  in (13) is symmetric and thus diagonalizable, so it has real eigenvalues and admits a basis of real orthogonal eigenvectors. Here the largest real eigenvalue is isolated in Fig. 5B. The theory thus predicts that the corresponding spectral component (solid line in Fig. 5C) dominates the dynamics and is potentiated, whereas the remaining ones are depressed. Numerical simulation using log-STDP agrees with this prediction, as illustrated in Fig. 5E. By gradually potentiating the correlated inputs, weight-dependent STDP results in a multimodal weight distribution that can better separate the mean weights of the pools. The final weight structure in Fig. 5F reflects the dominant eigenvector. Despite the variability of individual weight traces in Fig. 5D due to the noise in the weight update and rather fast learning rate used here, the emerging weight structure remains stable in the long run.

### Spike transmission after learning

Following the specialization induced by STDP, the modified weight distribution tunes the transient response to the input spikes. To illustrate this, we examine how STDP modifies the neuronal response to the three correlation sources  $\mathcal{R}_k$  in the previous configuration in Fig. 5. Practically, we evaluate the firing probability during a given time interval of  $D$  ms consecutive to a spike from input  $i$ , similar to a peristimulus time histogram (PSTH). Before learning, the PSTHs for  $\mathcal{R}_1$  (red),  $\mathcal{R}_2$  (green) and  $\mathcal{R}_3$  (blue) are comparable in Fig. 6A, which follows because  $\sqrt{c_1^1} + \sqrt{c_1^3} = 0.95$ ,  $\sqrt{c_2^2} + \sqrt{c_2^3} = 0.89$  and  $\sqrt{c_3^3} + \sqrt{c_4^3} = 0.63$ .

After learning, pools  $\bar{1}$  and  $\bar{2}$  that relate to  $\mathcal{R}_1$  and  $\mathcal{R}_2$  are much more potentiated than pool  $\bar{4}$  by STDP in Fig. 5F. Consequently, even though pool  $\bar{3}$  is potentiated and transmits correlated activity from  $\mathcal{R}_3$ , the spike transmission after learning is clearly stronger for  $\mathcal{R}_1$  and  $\mathcal{R}_2$  than  $\mathcal{R}_3$  in Fig. 6B. The respective increases of the areas under the PSTHs are summarized in Fig. 6C. The overall increase in firing rate (from about 10 to 30 sp/s) is not supported equally by all  $\mathcal{R}_k$ .

To further quantify the change in spiking transmission, we evaluate the mutual information  $MI$  based on the neuronal firing probability, considering correlated events as the basis of information. In this way, the increases in PSTHs are compared to the background firing of the neuron, considered to be noise. In contrast to previous studies that examined optimality with respect to limited synaptic resources [30,31], we only examine how STDP tunes the transmission of synchronous spike volleys. We define  $MI$  with respect to the event 'the neuron fires two spikes or more within the period  $D$ ', denoted by  $F$ ;  $\neg F$  is its complementary. Hereafter, we denote by  $\mathcal{R}_k$  and  $\neg\mathcal{R}_k$  the occurrence of a correlated event and its complementary, respectively. The mutual information is defined as

$$MI = \sum_{x,r} \Pr\{x,r\} \log_2 \left[ \frac{\Pr\{x,r\}}{\Pr\{x\} \Pr\{r\}} \right], \quad (14)$$

with  $r \in \{\mathcal{R}_k, \neg\mathcal{R}_k\}$  and  $x \in \{F, \neg F\}$ . The probabilities are defined for the events occurring during a time interval  $D$ . We have

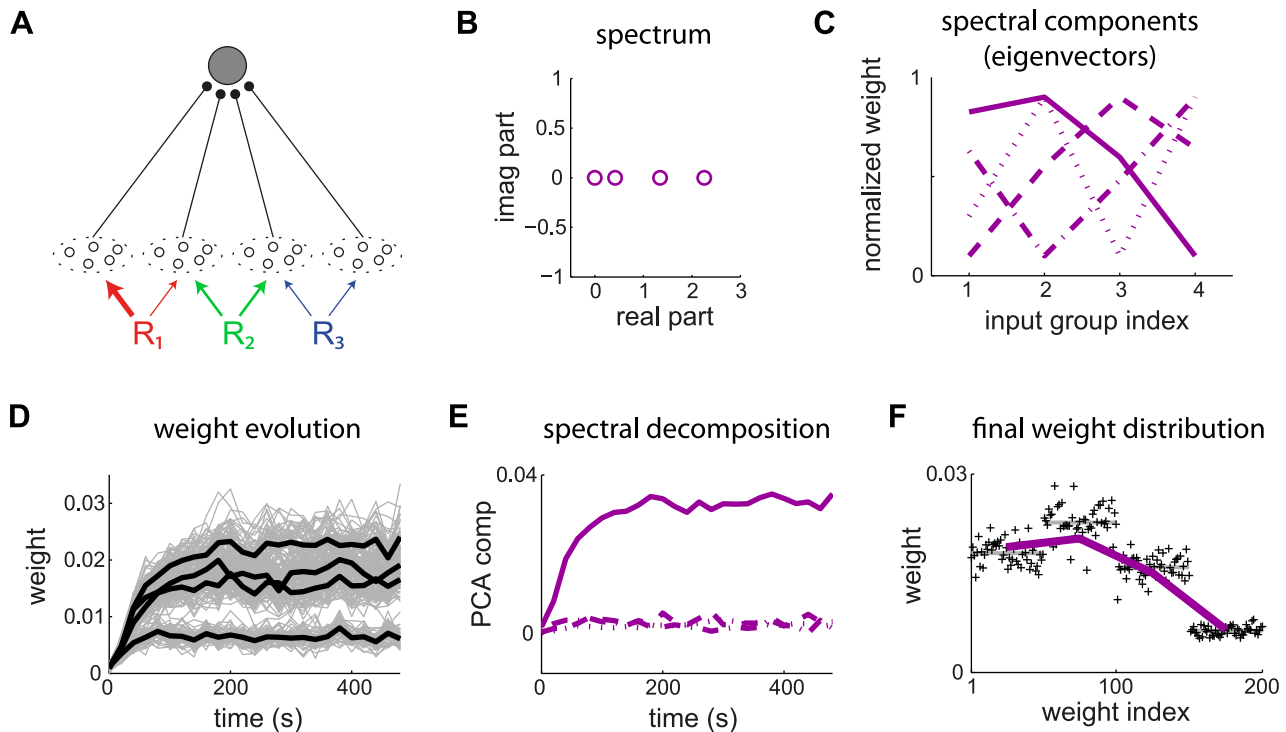


**Figure 5. Principal component analysis for mixed correlation sources.** (A) The postsynaptic neuron is excited by  $m=4$  pools of 50 inputs each with the global input correlation matrix  $C^Z(w^*)$  in (13). The thickness of the colored arrows represent the correlation strengths from each reference to each input pool. The input synapses are modified by log-STDP with  $\alpha=5$ . The simulation parameters are given in Table 1. (B) Spectrum and (C) eigenvectors of  $C^Z(w^*)$ . The eigenvalues sorted from the largest to the smallest one correspond to the solid, dashed, dashed-dotted and dotted curves, respectively. (D) Evolution of the weights (gray traces) and the means over each pool (thick black curves) over 500 s. (E) Evolution of the weights  $w$  in the basis of spectral components (eigenvectors in C). (F) Weight structure at the end of the learning epoch. Each weight is averaged over the last 100 s. The purple curve represents the dominant spectral component (solid line in C). doi:10.1371/journal.pcbi.1002584.g005



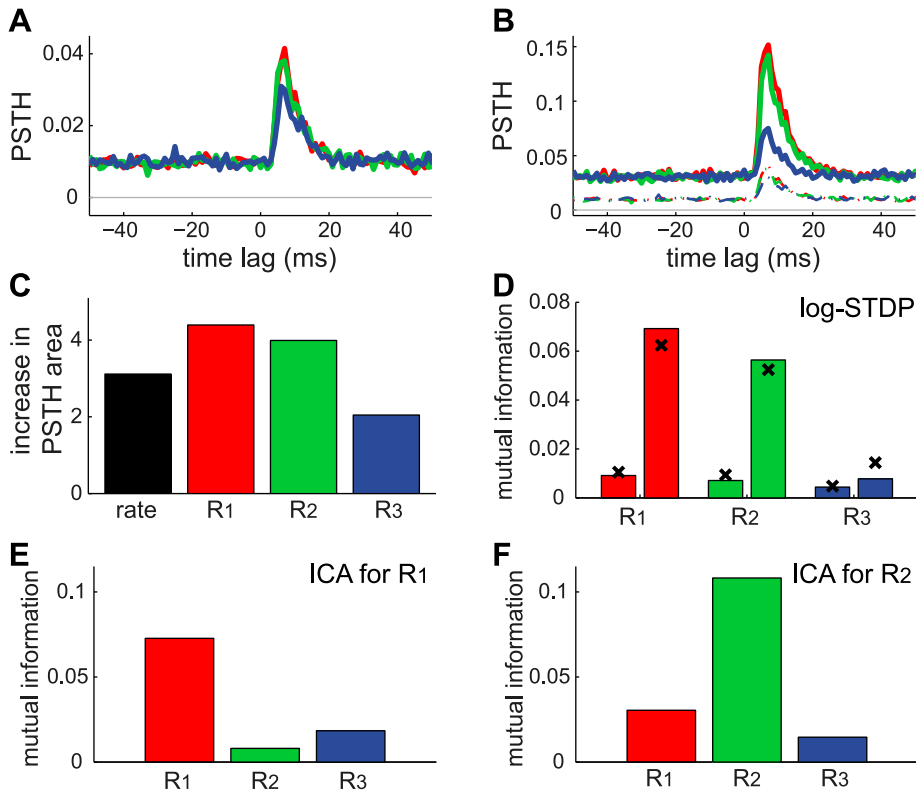


**Figure 6. Transmission of the correlated activity after learning by STDP.** The results are averaged over 10 neurons and 100 s with the same configuration as in Fig. 5. Comparison of the PSTHs of the response to each correlated event of  $\mathcal{R}_k$  (A) before and (B) after learning for  $k=1$  (red),  $k=2$  (green) and  $k=3$  (blue). Note the change of scale for the y-axis; the curves in A are reproduced in B in dashed line. (C) Ratio of the learning-related increase of mean firing rate (black) and PSTHs in B with respect to A (same colors). For each PSTH, only the area above its baseline is taken into account. (D) Mutual information  $MI$  between a correlated event and the firing of two spikes, as defined in (14). For each reference, the left (right) bar indicates  $MI$  before (after) learning. The crosses correspond to the theoretical prediction using (16) as explained in the text. (E) Example of neuron selective to  $\mathcal{R}_1$  with weight means for each pool set by hand to  $\bar{w}_1=0.03$ ;  $\bar{w}_2=\bar{w}_4=0.015$  and  $\bar{w}_3=0$ . The bars correspond to the simulated  $MI$  similar to D. (F) Same as E with a neuron selective to  $\mathcal{R}_2$  and  $\bar{w}_1=0.005$ ;  $\bar{w}_2=\bar{w}_3=0.03$  and  $\bar{w}_4=0$ . doi:10.1371/journal.pcbi.1002584.g006

$\Pr\{\mathcal{R}_k\} = v_0 D$  and the realization of  $F$  can be evaluated using a Poisson random variable with intensity  $\lambda$

$$\Pr\{\neg F|r\} = \frac{1+\lambda}{\exp(\lambda)}. \quad (15)$$

In the above expression,  $\lambda$  can be evaluated via the baseline firing rate for  $r = \neg\mathcal{R}_k$  and the PSTHs in Fig. 6B for  $r = \mathcal{R}_k$ . Namely, we adapt (48) and (49) in Methods to obtain

$$\lambda \simeq \begin{cases} Dv_{\text{out}}^* & \text{for } r = \neg\mathcal{R}_k \\ Dv_{\text{out}}^* + \sum_m N_m \sqrt{c_m^k} \bar{w}_m & \text{for } r = \mathcal{R}_k \end{cases}. \quad (16)$$

Using the simulation results for the mean  $\bar{w}_m$  and  $v_{\text{out}}^*$  we obtain the predicted values (crosses) for  $MI$  in (14) in Fig. 6D. They are in reasonable agreement with  $MI$  evaluated from the simulated spike trains after dividing the 100 s duration in bins of lengths  $D$ . In a clearer manner than with the ratio in Fig. 6C,  $MI$  shows that the strong potentiation induced by STDP leads to the reliable transmission (considering that Poisson neurons are noisy) of the correlated events involved in the strong spectral component of  $\mathcal{C}^Z$ , namely  $\mathcal{R}_1$  and  $\mathcal{R}_2$ , while that for  $\mathcal{R}_3$  remains poor.

For the input firing rate  $v_0 = 10$  sp/s used here, STDP potentiates the weights such that the postsynaptic neuron fires at  $v_{\text{out}} \simeq 30$  sp/s after learning. Because the frequency of correlated events for each source  $\mathcal{R}_k$  is also 10 times per second,  $MI$  is not so high in our model. Perfect detection for  $\mathcal{R}_1$  corresponds to firing three spikes for each corresponding correlated event and none otherwise. In this case,  $\Pr\{\mathcal{R}_k, F\} = \Pr\{F\} = \Pr\{\mathcal{R}_k\} = v_0 D$ ,  $\Pr\{\neg\mathcal{R}_k, \neg F\} = \Pr\{\neg F\} = \Pr\{\neg\mathcal{R}_k\} = 1 - v_0 D$  and  $\Pr\{\mathcal{R}_k, \neg F\} = \Pr\{\neg\mathcal{R}_k, F\} = 0$ , yielding the maximum  $MI = -v_0 D \log_2 [v_0 D] - (1 - v_0 D) \log_2 [1 - v_0 D] \simeq 0.81$ . In comparison, for  $v_0 = 5$  sp/s and the baseline log-STDP with  $\alpha = 5$  (results not shown), the firing rate after training is roughly eightfold that before learning. Then,  $MI \simeq 0.15$  for  $\mathcal{R}_1$  instead of about 0.07 in Fig. 6. For the Poisson neuron especially, high firing rates lead to poor  $MI$  because of the noisy output firing rate. Performance can be much enhanced by using inhibition [9], but we will not pursue optimal detection in the present paper.

#### From PCA to ICA: influence of STDP properties on input selectivity

The high neuronal response to both correlation sources in Fig. 6C arises because pools 1, 2 and 3 in Fig. 5F exhibit strong weights, in a similar manner to the example with Oja's rule in

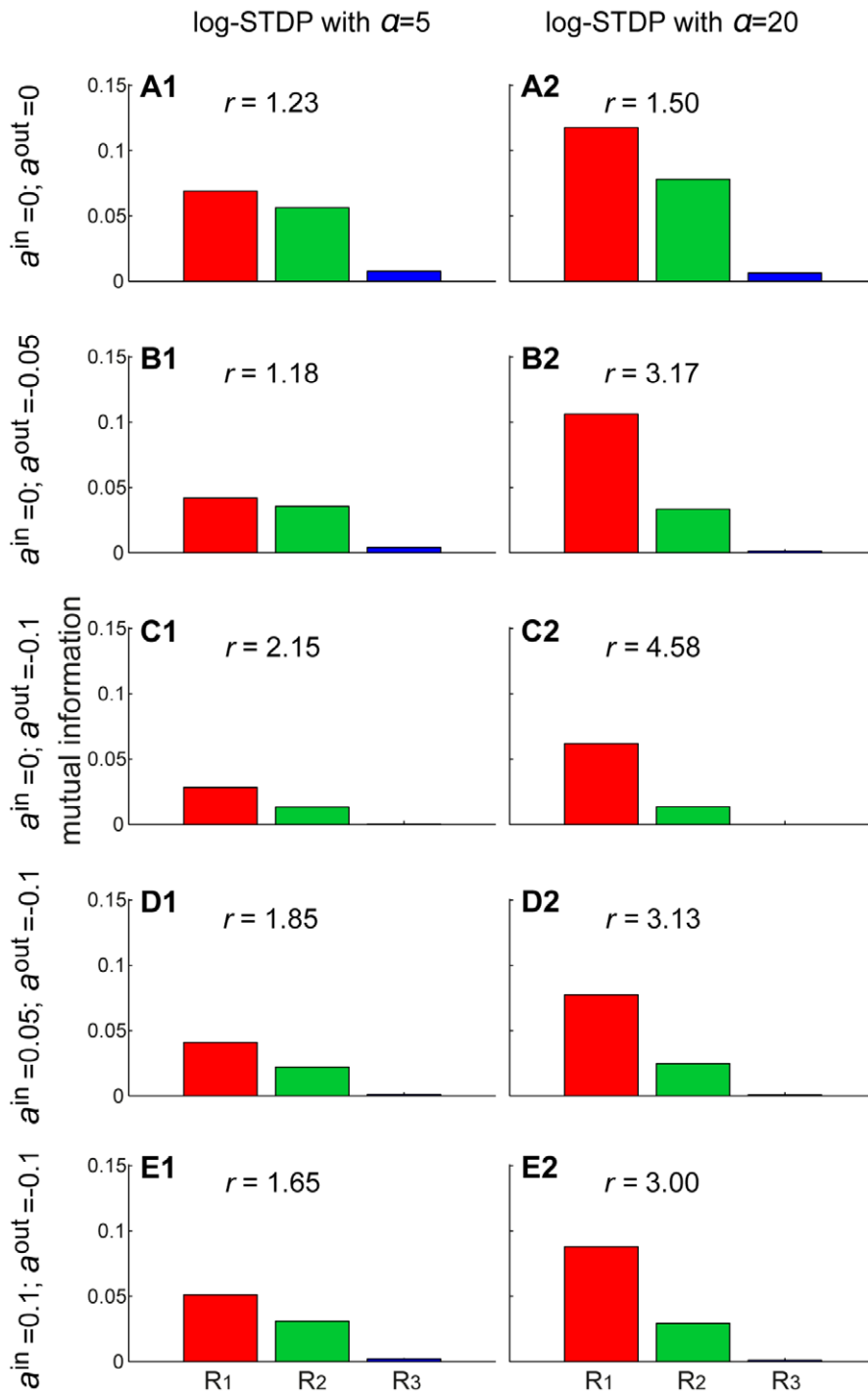


**Figure 7. From PCA to ICA.** The plots show the mutual information between each correlation source  $\mathcal{R}_k$  and the neuronal output firing after learning as in Fig. 6D–F. The neuron is stimulated by  $m=4$  pools that mix three correlation sources as in Fig. 5. The two columns compare log-STDP with different degrees of weight dependence: (1)  $\alpha=5$  and (2)  $\alpha=20$  that induces stronger competition via weaker LTD. Each row corresponds to a different combination of single-spike contributions: (A) plain log-STDP meaning  $a^{\text{in}} = a^{\text{out}} = 0$  and log-STDP+SCC with (B)  $a^{\text{in}} = 0$  and  $a^{\text{out}} = -0.05$ ; (C)  $a^{\text{in}} = 0$  and  $a^{\text{out}} = -0.1$ ; (D)  $a^{\text{in}} = 0.05$  and  $a^{\text{out}} = -0.1$ ; (E)  $a^{\text{in}} = 0.1$  and  $a^{\text{out}} = -0.1$ . The scale on the y-axis is identical for all plots. The ratio of  $MI$  between  $\mathcal{R}_1$  and  $\mathcal{R}_2$  is indicated by  $r$ . doi:10.1371/journal.pcbi.1002584.g007

Fig. 1D). However, it is possible to obtain a much better neuronal selectivity to either  $\mathcal{R}_1$  or  $\mathcal{R}_2$ , as illustrated in Fig. 6E–F for two distributions set by hand. The corresponding mean weights were chosen such that  $\mathbb{Q}\mathbf{w}^T$  favors the desired correlation source compared to others under the constraint of positive weights; cf.  $\mathbb{Q}$  in (12) and  $\mathbf{T}$  indicates the matrix transposition. We use mutual information as a criterion to evaluate whether kSCA resembles PCA or ICA [33]. Here the analysis of independent spectral component for the postsynaptic neuron means a strong response to *only* one correlation source in terms of  $MI$ .

To separate correlation sources as in Fig. 6E–F, stronger competition between the synaptic inputs is necessary. When tuning the weight dependence of log-STDP toward an additive-like regime, input weights corresponding to the dominant spectral component are more strongly potentiated. This increase results in higher  $MI$  with  $\alpha=20$  in Fig. 7A2 for both  $\mathcal{R}_1$  and  $\mathcal{R}_2$ , as compared to  $\alpha=5$  in Fig. 7A1. However, the neuron still responds strongly to  $\mathcal{R}_2$  in addition to  $\mathcal{R}_1$ , as indicated by the ratio  $r$  between the respective  $MI$ . So long as STDP causes the weights to specialize in the direction of the dominant spectral component, pool  $\bar{2}$  is the most potentiated and the neuron does not isolate  $\mathcal{R}_1$ . Even for log-STDP with  $\alpha=100$  or add-STDP (not shown), we obtain  $r \leq 1.6$ . This follows because of the positive input correlations used here. We need a mechanism that causes inputs excited by distinct correlation sources to compete more strongly to drive the neuron. The synaptic competition induced by a negative postsynaptic single-spike contribution  $a^{\text{out}} < 0$  satisfactorily increases the ratio  $r$  in Fig. 7B–C compared to A (except for B1). One drawback is that the larger negative  $a^{\text{out}}$  is, the smaller the mean equilibrium weight become, cf. (6). Consequently, even though the ratio  $r$  increases,  $MI$  decreases and the transmission of correlations is weakened. To compensate and obtain sufficiently large weights after learning, one can use a positive presynaptic single-spike contribution  $a^{\text{in}} > 0$ . This gives both  $MI$  for  $\mathcal{R}_1$  and large ratios  $r$  in Fig. 7D2–E2, but not in Fig. 7D1–E1. We conclude that, in order that the neuron performs ICA and robustly selects  $\mathcal{R}_1$ , STDP itself should also be sufficiently competitive to obtain robust selectivity, see Fig. 7B–E with  $\alpha=20$  compared to  $\alpha=5$ . By homogeneously weakening all weights after each output spike in addition to strong STDP-based LTP, only the inputs that most strongly drive the output firing remain significantly potentiated. In other words,  $a^{\text{out}} < 0$  introduces a threshold-like effect on the correlation to determine which inputs experience LTP and LTD. In agreement with our prediction, this “dynamic” threshold becomes more effective for large output firing rates, which only occurs when STDP leads to strong LTP ( $\alpha=20$ ). This is reminiscent of BCM-like plasticity for firing rates [49]. Note that we found in simulation (not shown) that using  $a^{\text{in}} > 0$  alone did not lead to ICA; this only increases the mean input weights.

To further examine the effect of STDP parametrization and assess the generality of our analysis, we examine common trends and discrepancies in the weight specialization for different schemes for weight dependence for plain STDP: log-STDP [16], nlta-STDP [13], mlt-STDP [38] and add-STDP [12]; as well as the influence of single-spike contributions with log-STDP+SCC, nlta-STDP+SCC and add-STDP+SCC [6]. We consider the configuration represented in Fig. 8A where two sources of correlation excite three pools among four. The third pool from the left is stimulated by the same source as the second pool after a time lag of 20 ms. The corresponding spectrum of  $\mathbb{C}^Z$  is given in Fig. 8C, leading to two dominant spectral components with equal real part, one for each correlation source. Due to the large imaginary parts of the complex conjugate eigenvalues related to  $\mathcal{R}_2$ , the final distribution in Fig. 8D does not reflect the green component in the

sense that pool  $\bar{3}$  is not potentiated, but depressed. This follows because its correlated stimulation comes late compared to pool  $\bar{2}$ . Therefore, the weights from pool  $\bar{3}$  become depressed when the weights from pool  $\bar{2}$  become large. The final weight evolution differ from the initial splitting whereas both weight sets grew (not shown), as expected by the theory. For log-STDP, the weight dependence regulates the number of selected components. Both red and green components are represented in Fig. 8D, whereas the green component dominates in Fig. 8E. Nlta-STDP can also generate graded distribution as log-STDP does. The synaptic competition in Fig. 8G is comparable to that in Fig. 8E. In comparison, mlt-STDP induces weaker competition, although the asymptotic weights reflect the spectral components in Fig. 8I. On the other hand, add-STDP in Fig. 8J generates a bimodal distribution of weights, which is a thresholded version of Fig. 8D,E or G.

In the case of add-STDP+SCC, the neuronal selectivity is controlled via the equilibrium mean weight  $w_{\text{av}}^*$  that is constrained by the single-spike contributions  $a^{\text{in/out}}$  in (6). The situation is more complex for weight-dependent STDP+SCC, as the kernels  $\chi(w_i, \tau)$  is modified by as the weights evolve. Nevertheless, similar effects were observed in simulations. For log-STDP+SCC (Fig. 8F) and nlta-STDP+SCC (Fig. 8H), the qualitative profile of the final weights is similar to that for plain STDP, with the additional competition induced by  $a^{\text{out}} < 0$  that depresses pool  $\bar{1}$  and favors  $\bar{2}$ , as was described in Fig. 7. In the case of add-STDP+SCC, the instability of the dynamics leads to more sensitivity to the single-spike contributions. With  $a^{\text{in}}=0.1$  and  $a^{\text{out}}=-0.1$  in Fig. 8K, only the weights from pool  $\bar{2}$  are potentiated at the end of the learning epoch. However, with  $a^{\text{in}}=0.15$  and  $a^{\text{out}}=-0.02$  in Fig. 8L, the competition is weakened and all weights from pools  $\bar{1}$  and  $\bar{2}$  are potentiated, in agreement with the theoretical prediction. Interestingly, some weights from the uncorrelated pool  $\bar{4}$  are mildly potentiated, whereas those from the positively correlated pool  $\bar{3}$  are more strongly depressed toward zero because of the time lag associated to  $\mathcal{R}_2$ .

### Influence of the postsynaptic response

Now we examine how the postsynaptic response affects the weight competition. This turns out to be particularly important when the correlograms have a temporal extension, that is, richer than just narrowly correlated inputs with a peak at  $\tau=0$ . We consider the configuration in Fig. 9A where inputs from the pool  $\bar{1}$  tend to fire a time lag  $\Delta=10$  ms before those of pool  $\bar{2}$ . Namely, correlation is generated following (11) using a reference  $\mathcal{R}^1$  with  $\mathcal{I}_{i,1}^1=0$ ,  $\mathcal{I}_{j,1}^1=\Delta$ , and  $\bar{c}_{i,1}^1=\bar{c}_{j,1}^1=\bar{c}=0.1$ . Pool  $\bar{3}$  has no correlation. The matrix  $\mathbb{C}^Z$  in (3) averaged over pools is not symmetric:

$$\bar{\mathbb{C}}^Z(w_{\text{av}}^*) = \bar{c}v_0 \begin{pmatrix} \chi(w_{\text{av}}^*, 0) & \chi(w_{\text{av}}^*, \Delta) & 0 \\ \chi(w_{\text{av}}^*, -\Delta) & \chi(w_{\text{av}}^*, 0) & 0 \\ 0 & 0 & 0 \end{pmatrix}. \quad (17)$$

Following (4), the PSPs and delays affect the kernel  $\chi$  (here identical for all synapses), hence  $\mathbb{C}^Z(\mathbf{w}^*)$  and the resulting weight selection. In Fig. 3C, the same STDP learning window is combined with different PSP kernels and synaptic delays. We first use the baseline parameters in Fig. 9B1: a rise constant  $\tau_A=1$  ms and a decay constant  $\tau_B=5$  ms for the PSP kernel and purely axonal delays  $d_i^{\text{ax}}=5$  ms. They correspond to the blue curve in Fig. 3C. In this case, the matrix  $\mathbb{C}^Z(w_0)$  may be rather antisymmetric (outside its diagonal):

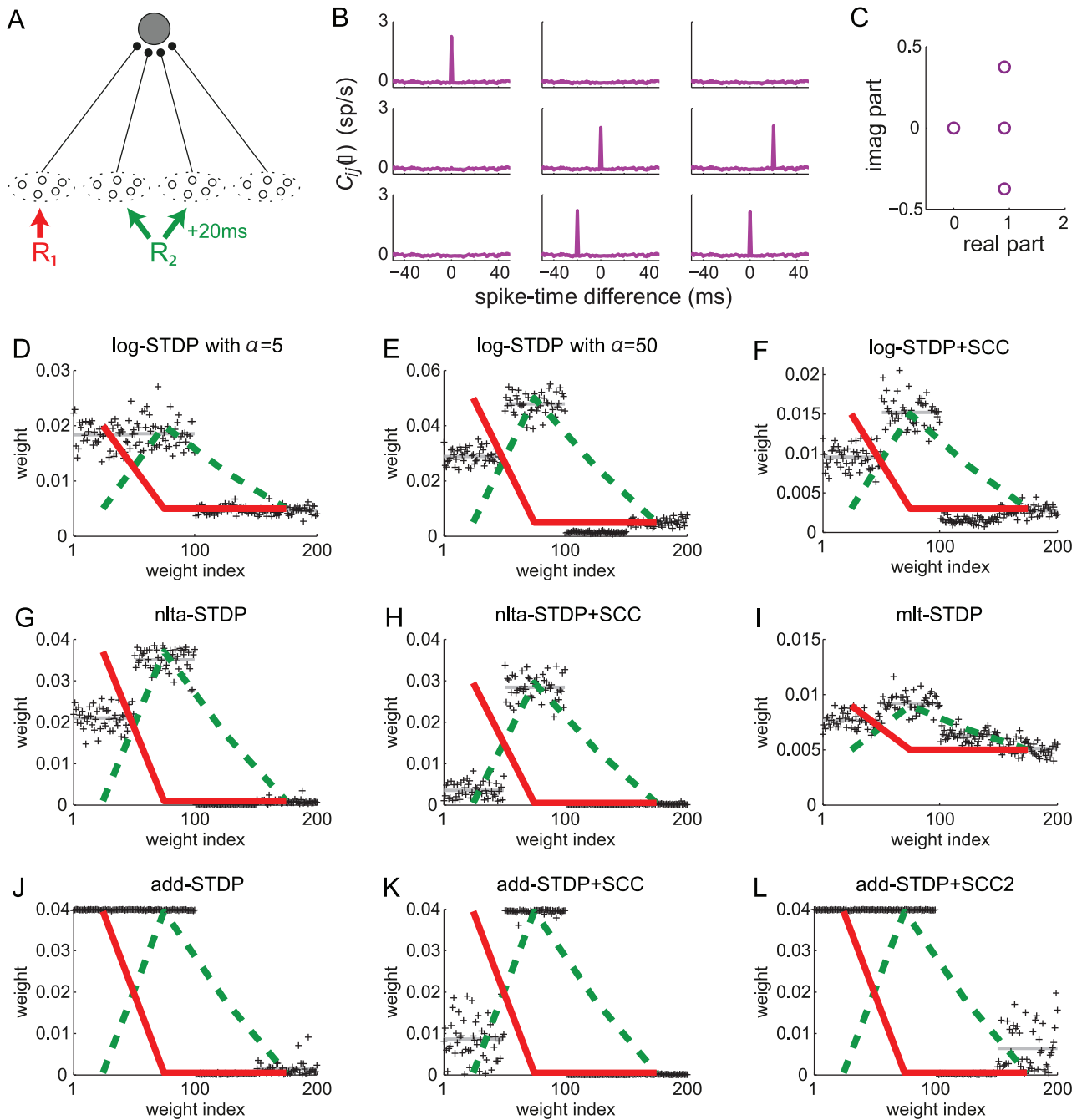


**Figure 8. Influence of the STDP parameters.** (A) The neuron is stimulated by four pools. From left to right, pool 1 is stimulated by the correlation source  $\mathcal{R}_1$  with correlation strength  $c_1^2 = 0.25$  in (11). Pools 2 and 3 are related to the correlation source  $\mathcal{R}_2$  with  $c_2^2 = c_3^2 = 0.25$ ; pool 3 tends to fire  $\bar{t}_3 - \bar{t}_2 = 20$  ms after pool 2. (B) Input cross-correlograms  $C_{ij}(\cdot, \tau)$  for first three pools described in A. The simulation time is 1000 s and the spike counts have been rescaled by the time bin equal to 1 ms. The peak is predicted by (11). Note the shift of the peak for the cross correlograms between inputs from pools 2 and 3. (C) Spectrum of the correlation matrix  $C^X$  corresponding to B. (D–L) Comparison of the final weight distribution for different STDP models. The two strongest spectral components of the correlation structure in red and green thick lines; they are rescaled between the minimum and maximum weights obtained in the simulation. For STDP+SCC in F, H and K, the single-spike contributions are  $a^{\text{in}} = 0.1$  and  $a^{\text{out}} = -0.1$ . (D) log-STDP with  $A_+ = 1$ ,  $A_+ = 0.5$  and  $\alpha = 5$ ; (E) log-STDP as in D with  $\alpha = 50$ ; (F) log-STDP+SCC with the same parameters as D; (G) nlta-STDP with  $A_+ = 1$ ,  $A_+ = 0.8$  and  $\gamma = 0.1$ ; (H) nlta-STDP+SCC with the same parameters as G; (I) mlt-STDP with  $A_+ = 1$ ,  $A_+ = 100$  (J) add-STDP with  $A_+ = 1$ ,  $A_+ = 0.55$ ; (K) add-STDP+SCC with the same parameters as J; (L) add-STDP+SCC2 with  $a^{\text{in}} = 0.15$  and  $a^{\text{out}} = -0.02$ .  
doi:10.1371/journal.pcbi.1002584.g008

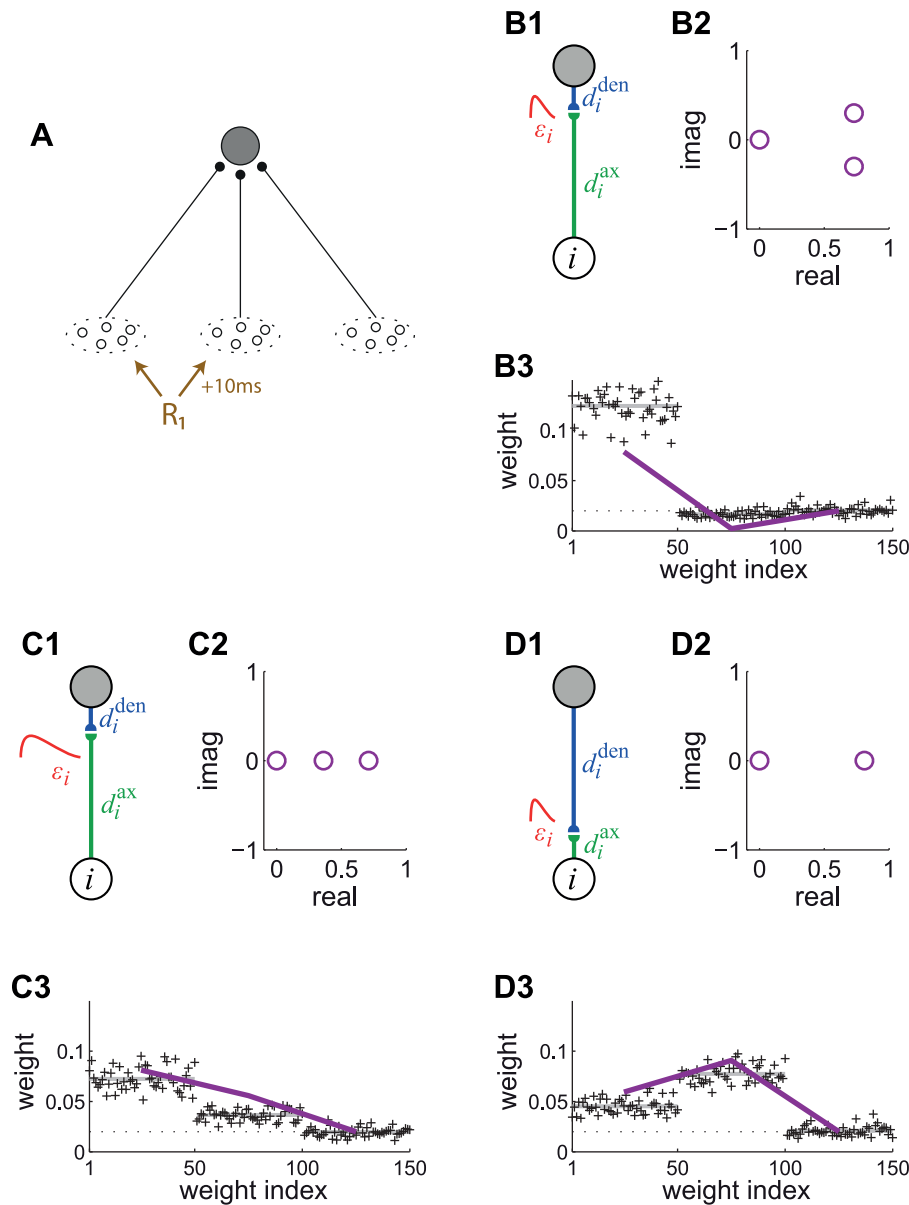


**Figure 9. Influence of the PSP response on the kernel  $\chi$  and the resulting weight structure for log-STDP.** (A) The neuron is stimulated by  $m=3$  input pools. The first two pools have the same reference for correlations with strength  $\bar{c}=0.1$  and pool 2 tends to fire  $\Delta=10$  ms after pool 1. Pool 3 has no correlation. For all inputs, the firing rate is  $v_0=5$  sp/s. (B) Short PSP response with  $\tau_A=1$  ms and  $\tau_B=5$  ms, as well as purely axonal delays  $d_i^{ax}=5$  ms. (C) Long PSP response with  $\tau_A=3$  ms and  $\tau_B=10$  ms, as well as purely axonal delays  $d_i^{ax}=5$  ms. (D) Short PSP response with  $\tau_A=1$  ms and  $\tau_B=5$  ms, as well as purely dendritic delays  $d_i^{den}=5$  ms. For each configuration, we present (1) a schematic diagram of the synaptic parameters, (2) the eigenvalues of  $\bar{C}^Z(w^*)$  and (3) the resulting weight specialization. As in Fig. 5, the purple curves represent the expression in (10). The dotted horizontal line indicates  $w_0$ , the equilibrium weight for log-STDP. Two eigenvalues are roughly equal to zero in D2. doi:10.1371/journal.pcbi.1002584.g009

$$\bar{C}^Z(w_0) \sim \begin{pmatrix} + & - & 0 \\ + & + & 0 \\ 0 & 0 & 0 \end{pmatrix}, \quad (18)$$

cf. the values of the blue curve indicated by the arrows in Fig. 3C. The eigenvalues are represented in Fig. 9B2. This indicates that the (correlated) pool 2 fires “late” with respect to pool 1, from the point of view of STDP. It follows that the second pool is depressed while the first pool is potentiated, as illustrated in Fig. 9B3.

In contrast, a different weight selection occurs for the same axonal delays, but longer PSP time constants in Fig. 9C:  $\tau_A=3$  ms,  $\tau_B=10$  ms (the purple curve in Fig. 3C); as well as dendritic delays  $d_i^{den}=5$  ms with the same short PSP time constants in Fig. 9D (green curve in Fig. 3C). In both cases, this follows because  $\bar{C}^Z(w_0)$  has the following form:

$$\bar{C}^Z(w_0) \sim \begin{pmatrix} + & + & 0 \\ + & + & 0 \\ 0 & 0 & 0 \end{pmatrix}, \quad (19)$$

which is “more” symmetric compared to Fig. 9B, and thus does not depress the late pool. The change in  $\chi_i$  affects the spectrum, which results in the potentiation of both correlated pools  $\bar{1}$  and  $\bar{2}$ , as illustrated in Fig. 9C2 and D2. For the case of a delay of the dendritic delay in Fig. 9D3, the late pool  $\bar{2}$  is more strongly potentiated than the early pool  $\bar{1}$  as  $\chi(w_{av}^*, \Delta)$  corresponds to the peak of the kernel, cf. the right arrow and the green curve in Fig. 3C. This illustrates that the effect of pool  $\bar{1}$  on the output firing felt at the synapse (i.e., after twice the dendritic delay  $d_i^{\text{den}} = 5$  ms) coincides with the firing of pool  $\bar{2}$ , namely 10 ms after pool  $\bar{1}$ .

## Discussion

We have demonstrated how the STDP dynamics reflect the spectral properties of temporal correlations conveyed by input spike trains. The present analysis links the physiological properties of STDP, such as its learning window and weight dependence, to function in terms of spiking information. It sheds light on recent numerical studies [7,29] that used STDP to separate correlation sources, thus performing ICA. Such spectral decomposition capabilities appear to be the inherent algorithm of STDP. We find that, for a neuron with linear input-output response, excitatory pairwise STDP *alone* performs PCA-like computations. Weight-dependent STDP that induces both graded and robust LTP generates a rich representation of the input correlation structure. However, an additive-like weight dependence is not sufficient for ICA in general. In order to achieve ICA, STDP requires an additional homeostatic mechanism. Here we have used LTD triggered by single output spikes that prevents all weights from growing and results in enhanced competition between correlation sources.

### Input configuration and spectral components

For pairwise STDP, the weight dynamics can be predicted provided the firing rates and pairwise cross-correlations are well defined. The corresponding expressions (35) and (36) in Methods highlight the separation of timescales between rate-based and spike-based effects, which is determined by the learning window  $W$ . Spike-time correlations arise when coordinated firing between neurons is consistently repeated over time, such as a repeating spatiotemporal pattern embedded in random spiking activity and peaked PSTHs in experimental data. In the correlation structure induced by such pattern presentations, strong spectral components correspond to dense and peaked clusters of pattern spikes, in a similar fashion for both spike coordination and rate covariation [9]. Our framework can account for a rich variety of input configurations, in particular, stimuli that were used with STDP for categorization and/or representation in previous studies [8–10,50–52], as well as recently proposed elaborate input configurations [46–48]. Time-varying signals can also generate significant spike-time correlations and thus weight specialization (Text S2 and Fig S2).

### Kernel spectral component analysis (kSCA) of input spike-time correlations

The present framework aims to provide a unified description of the STDP dynamics for the many configurations that have been used in previous studies. Following the observations by Gerstner and Kistler [25, Ch~11], STDP potentiates and depresses weights depending on the spectral components of  $\mathbb{C}^\chi$ . This matrix embodies the STDP-specific effects and is determined by the input correlation structure  $\mathbb{C}$  and kernels  $\chi$ . The kernels are

determined by the STDP learning window and PSP responses, cf. (4). In a sense, the cross-correlograms in  $\mathbb{C}$  are “seen” by the neuron through the kernels  $\chi$ . This is especially important when input correlograms have a temporal extension (Fig. 9) or when the shape of the STDP learning window function  $W$  varies across synapses. When using long timescales for PSPs with usual time constants for the learning window  $W$ , the matrix  $\mathbb{C}^\chi$  tends to be symmetric and the PCA performed by STDP can result in slow-feature extraction [27]. Another point is that the input correlation structure as a *whole* determines for the weight specialization. In Fig. 8L for example, uncorrelated inputs are not as depressed by STDP as some positively correlated inputs. The present study has focused on Hebbian STDP for excitatory synapses (Fig. 2C), but the same framework can be used for any arbitrary learning window  $W$ , as well as the case of plastic inhibitory synapses [53]. A neuron can thus generate elaborate representations of the stimulating inputs in its weight structure, which illustrates the versatility of STDP.

**Relationship to Oja’s rule.** When the input configuration corresponds to mixed instantaneous correlations, STDP alone can perform PCA on the correlation strengths (Fig. 5). In this way, STDP can be seen as an extension of Oja’s rule [24], as was suggested by van Rossum et al. [26]. There are several important differences, though:

- Oja’s rule relies on rate-based information, which implies a symmetric cross-correlation matrix between inputs and thus performs PCA (Fig. 1). STDP, however, is based on the spike-time correlograms contained in  $\mathbb{C}(\cdot, \tau)$ . The matrix  $\mathbb{C}^\chi$  is determined by the kernels  $\chi_i$  (Fig. 3) and may thus not be symmetric, especially for the usual temporally Hebbian learning window  $W$ . This implies richer weight specialization via the interaction with the neuronal parameters (Fig. 9).
- When the eigenvalues have large imaginary parts (Fig. 8), the final weight distribution may not reflect the initial weight splitting. Nevertheless, the weights that win the synaptic competition, in the sense of being eventually most strongly potentiated, are satisfactorily predicted by (10).
- In addition to the first Hebbian term in (1), the second term in Oja’s rule leads to a specific constraint that drives the weights toward the principal spectral component. When STDP performs PCA-like computations, adequate weight dependence resulting in graded LTP results in a better representation of the principal component (Figs. 5 and 8).
- For STDP, the resulting neuronal selectivity is determined by the weight dependence, as well as the additional homeostatic mechanisms. This allows flexibility in tuning the learning process. For example, STDP can also switch from PCA to ICA, as will be discussed in more depth below. In contrast, more than one spectral component of  $\mathbb{C}^\chi$  can be selected when the competition is not too strong (Fig. 8D). On the other hand, Oja’s rule requires several neurons to extract several spectral components, as each neuron only selects a single component.

**Influence of weight dependence.** When STDP performs PCA, a desirable outcome is a fine representation of the main spectral component of the input covariance in the weight structure. When the weight evolution is consistent with the initial splitting, the final weight distribution reflects the principal component in (10), as illustrated in Figs. 5F and 9. The key is a graded potentiation of correlated inputs as induced by log-STDP [13] or nlta-STDP [16]. This functional property of the experimentally observed weight dependence complements previous conclusions about its role in regulating the synaptic

competition and shaping the weight distribution [13,15,16,38,39]. To obtain effective weight specialization, STDP should be parametrized in an additive-like regime. However, purely additive STDP often leads to a bimodal distribution of synaptic weights, which may not reflect the complexity of the input structure. In addition, we have observed that add-STDP can lead to unstable synaptic dynamics over an extended learning epoch. Figure S1C provides an example of quasi-periodic evolution of the synaptic weights when  $\mathbb{C}^Z$  has dominant eigenvalues with large imaginary parts. Even a slight dose of weight dependence appears sufficient to introduce stability in the weight dynamics in this case (Fig S1D), which agrees with the existence of a fixed point predicted by our analysis.

**From PCA to ICA.** An important conclusion of our results is that kSCA performed by *plain* STDP relates to PCA, but differs from ICA. For example, the dominant component of the input correlations in Fig. 5 mixes the correlations from  $\mathcal{R}_1$  and  $\mathcal{R}_2$ . So long as STDP potentiates the weights in that “direction”, the trained neuron does not become selective to only *one* correlation source. However, additional constraints on the weight dynamics can disrupt this scheme. As shown in Fig. 7, when the additional competition induced by  $a^{\text{out}} < 0$  [6] is sufficiently strong, the neuron can become selective to a single correlation source by tuning its positive synaptic weights. This results in a winner-take-all situation for the strongest correlation source involved in the dominant spectral component. This competitive effect complements the homeostatic regulation on the mean weight by the pre- and postsynaptic single-spike contributions [35]. The neuronal selectivity in Figs. 6 and 7 is measured using the mutual information between input correlated events and output firing. This provides a suitable criterion to discriminate between PCA and ICA [33] and has been used to evaluate the performance of STDP in extracting information within noisy spike trains [30–32].

There exist configurations where PCA and ICA coincide, for example, when each spectral component (eigenvector) is associated with a single correlation source (Fig. 8A). Then, the selection of *one* eigenvector actually results in ICA. In such cases, pairwise STDP in a competitive (additive-like) regime can lead to a symmetry breaking, namely segregation between similar eigenvalue of  $\mathbb{C}^Z$  [13,16,17]; see also Fig. 8E compared to D. Therefore, we have used mixed correlation sources to investigate more carefully whether kSCA resembles PCA or ICA (Fig. 5), in a similar manner to Fig. 1 where the correlation sources overlap.

One issue with ICA in our model is that the performance crucially depends on the values  $a^{\text{in}}$  and  $a^{\text{out}}$ . For distinct input configurations, these values may have to be adjusted. Two opposing effects are operating here. First, The competition due to  $a^{\text{out}} < 0$  that brings ICA becomes stronger for increasing input correlation strength if the neuronal firing rate becomes stronger. Second, large negative values for  $a^{\text{out}}$  prevent the weights from being strongly potentiated, which leads to a low output firing rate. Further work is necessary to understand this interplay in more depth. An alternative to  $a^{\text{in/out}}$  to regulate the mean weight is a homeostatic weight scaling [38,54]. The precise nature of such a scaling critically affects the neuronal selectivity. When combined with rate-based Hebbian learning, subtractive normalization enables symmetry breaking, whereas multiplicative normalization leads to a form of PCA [55]. Previous studies that managed to perform ICA using STDP used a homeostatic weight scaling that normalizes the mean weight [29]. In an abstract learning model, Xu et al. [56] have demonstrated how such weight normalization constraints can cause the same update rule to switch between PCA and other algorithms such as ‘k-means’, i.e., grouping input pools

at distinct levels of potentiation (cf. Fig. 8J–K with the first two pools).

To achieve ICA with arbitrary input configurations with automatic tuning, adaptative nonlinearities in the neuronal response have been successfully used [29]. Such a nonlinear neuronal response captures higher-than-second-order correlations in a similar fashion to previous studies using rate-based learning [57]. Intuitively, superlinear PSP responses boost the competition between the weights, which prevents the output neuron from strongly responding to independent correlation sources. Likewise, STDP models relying on triplets of spikes can use such higher-order statistics to separate correlation sources [58]. Last, we have only considered positive weights here. The weights may be eventually potentiated or depressed compared to the mean equilibrium value for uncorrelated inputs (this difference is the equivalent of positive/negative weights in PCA in machine learning). Only significantly stronger weights transmit correlation patterns efficiently, whereas weaker weights hardly drive the postsynaptic neuron. Although ICA-like specialization can be achieved under the constraint of positive weights (Fig. 6E–F), inhibition can enhance the input selectivity when it strongly suppresses the transmission of certain correlation patterns [59].

### Extension to more elaborate STDP and neuron models

The present study has focused on STDP contributions up to the second order (pairs of pre- and postsynaptic spikes) and the learning dynamics that arise from the effect of pairwise spike-time correlations. This means that higher-order correlations only play a role via their collective second-order effects. In contrast, triplets or bursts of spikes can significantly modulate the weight updates in other models [40,60]. The model proposed by Appleby and Elliott requires multispike interactions (i.e., higher-order correlations) for synaptic competition to emerge [41]. More elaborate STDP models also present advantages for spike computation and/or reproducing experimental data [7,31,34,40,61,62]. In addition to the effect of spike-time correlations considered here, some of these models are sensitive to firing rates. Likewise, when spike pairs contributing to STDP are restricted (whereas all pairs are included in our model), the equilibrium mean weight depends on the input firing rates [4,5] and the balance between spike and rate effects is affected. Our results are expected to hold at least partially when pairwise effects dominate the STDP dynamics. Extending our study is left for subsequent work, but making use of higher-order correlations appears promising to perform ICA [58]. Although our STDP update incorporates noise, our analysis neglects it and assumes that the weight drift (i.e., mean change or first stochastic moment) dominates the dynamics. In extreme cases, a fast learning rate can compromise the stability of the emerged weight structure [14].

The present analytical study is based on the “linear” Poisson neuron, which allows a tractable analysis. Its stochastic firing mechanism generates rather noisy and unreliable spike trains compared to deterministic neuron model where the stochasticity arises from the inputs, e.g., integrate-and-fire neurons. Similar weight dynamics for both models have been demonstrated previously for slow STDP learning [6,13]. As mentioned above, a nonlinear firing response may be useful to perform ICA. In order to go beyond the linear input-output regime for integrate-and-fire neurons [63], it is necessary to study how the neuron model shapes the input-output covariance; see (32) in Methods. In most neuron models, larger excitatory weights induce stronger input-output correlations for correlated inputs. This results in a positive-feedback loop for learning, which is captured by the Poisson neuron model. Dendritic integration of synaptic inputs are expected to bring interesting nonlinearities to the kernel  $\chi$  defined in (4). Moreover,

depending on regional competition between and within dendritic branches [64,65], different components can be represented in distinct areas of a single neuron. Including such refinements opens promising ways to understand spike-based computations.

### Implications for spiking information processing in neuronal networks

Finally, our results support the idea that neurons equipped with STDP can operate as self-adapting filters that process information based on the transient firing response of neurons. The input-output spike-time covariance ( $F_i$  in our model) is simply the average of the transient response over all input statistics. STDP tunes these input-output correlations based on the input cross-correlation structure ( $\mathbb{C}^2$ ). Extending previous results focusing on a single correlated pathway [12], Fig. 6 illustrates the modification of the transmission of coincidentally spiking activity using mutual information as a measure of signal-to-noise. This view is consistent with the hypothesis that the coordinated activity of cell assemblies can serve as a basis for the neuronal code [66]. In a more general scheme, spiking information should also consider the detailed shapes of the correlograms, not just their integral value as here. Because of the temporal dimension, coding using correlations appears richer than rate-based coding, as was observed in experiments [67]. Propagation of coordinated transient spiking activity, which can be seen as a generalization of PSTHs or spike patterns [9], appears suitable for coding/decoding and naturally interacts with STDP. Depending on the more or less peaked shapes of the corresponding correlograms, the neurons may operate in either closer to a spike-based or a rate-based regime; these two forms of neuronal coding in feedforward networks are actually the two sides of the same coin [68]. Here correlations involve multiple input spike trains and all neurons belonging to the same assembly exhibit pairwise correlograms that have “coordinated” shapes, in a similar manner to cliques in graphs. Although a formal quantification has yet to be defined, the information in  $\mathbb{C}$  can intuitively be understood in terms of the diversity and arrangement of cross-correlograms. The kernels  $\chi_i$  then define a “similarity measure” on matrices  $\mathbb{C}$ : the respective shapes of the correlograms and kernels determine the effective strength of spectral components.

In a network, heterogeneity in the synaptic properties (PSP response and delays) and STDP learning windows leads to distinct kernels  $\chi$  among the synapses, so neurons can extract different components from a common input correlation structure. This can be used by (inhibitory) STDP to extract the frequency of rhythmic neuronal activity [53], which has been observed in many brain areas. Large inhomogeneities are expected to affect the weight specialization for oscillatory signals [10,11,45,69]. They may also play a role in encoding of slow signals at the shorter timescale of STDP [70,71]. Likewise, partial input connectivity allows neurons to see only part of the same global input structure, leading to differentiated specialization that may represent many spectral components. However, further developments are necessary to extend this analysis to the case of recurrent connections, which constrain the correlation structure [19], and incorporate possibly plastic inhibitory connections. This theory aims to better understand how neurons can process spiking information in a distributed fashion [72]. Interesting applications have been proposed recently [73,74]: STDP can preprocess temporal signals within a recurrently connected network that act as a (huge) reservoir of functions of the inputs, which enhances the performance of the so-called liquid state machine [75]. Cessac et al. also showed that STDP can change the network activity such that observables (e.g., firing rates, spiking synchrony) obey Gibbs

distributions [76]. Together, these efforts will hopefully lead to novel interpretations on how neurons can process spike trains.

## Methods

After the presentation of the STDP models, the following sections detail the derivation of the learning equation (2), which is analyzed in Results. The spike-time covariances of presynaptic spike trains, which is the crucial input information for the kSCA algorithm, are formally defined in a later section. Conditions on the existence of a stable fixed point for the weight dynamics are then derived. Finally, the neuronal response to input correlations is calculated in a simple case, which is used to evaluate theoretically the change in mutual information in Results.

### Phenomenological model of pairwise weight-dependent STDP

Pairs of pre- and postsynaptic spikes, as well as single spikes, completely determine the contributions to STDP. This choice has limitations compared to more elaborate models that include, for example, triplets or bursts of spikes in their analysis [40,69] or models for which pairwise correlations do not generate competition [41]. This choice allows us to focus on the next stochastic order after firing rates (first order) while keeping the analysis tractable.

For a pair of pre- and post-spikes whose effects reach the  $i$ th synaptic site at times  $t_i^{\text{pre}}$  and  $t_i^{\text{post}}$ , respectively, the weight  $w_i$  is modified by the following additive terms

$$\Delta w_i = \eta \begin{cases} a^{\text{in}} & \text{at time } t_i^{\text{pre}}, \\ a^{\text{out}} & \text{at time } t_i^{\text{post}}, \\ (1 + \zeta)W(w_i; t_i^{\text{pre}} - t_i^{\text{post}}) & \text{at time } \max(t_i^{\text{pre}}, t_i^{\text{post}}). \end{cases} \quad (20)$$

In general, we assume that the STDP-specific update  $W(w_i; t_i^{\text{pre}} - t_i^{\text{post}})$  depends on the current value of the weight  $w_i$  [13,38,39,42], in agreement with experimental evidence [37]. This weight dependence alone can stabilize the weight distribution for ‘plain STDP’, i.e., without single spike contributions. However, in the absence of weight dependence, single-spike contributions  $a^{\text{in/out}}$  are necessary to enforce partial stability on the weights, namely homeostasis on their mean [6,35,36]. Note that both mechanisms can also be successfully used together [15]. We will refer to the case where  $a^{\text{in/out}} \neq 0$  as ‘STDP+SSC’, in contrast to ‘plain STDP’ (or ‘STDP’ alone when there is no possible confusion) for  $a^{\text{in}} = a^{\text{out}} = 0$ . The second case is often regarded as more biologically plausible for excitatory STDP and will be the focus on this work. Although their effect is not considered in detail, the weight update in (20) involves a learning rate  $\eta$ , which determines the speed of learning, and variability in the pair-specific contribution, which is modeled by the white-noise random variable  $\zeta$  that has zero mean and variance  $\sigma$ .

As mentioned above, the contribution specific to spike pairs depends on the relative timing of pre- and postsynaptic spiking activity felt at the synaptic site. For the synapse  $i$  described in Fig. 2B, a pulse fired by the presynaptic neuron  $i$  at time  $t_i^{\text{pre}}$  and a pulse fired by the postsynaptic neuron at time  $t_{\text{out}}^{\text{post}}$  correspond to

$$\begin{aligned} t_i^{\text{pre}} &= t_i^{\text{n}} + d_i^{\text{ax}}, \\ t_i^{\text{post}} &= t_{\text{out}}^{\text{m}} + d_i^{\text{den}}. \end{aligned} \quad (21)$$

Typically for excitatory STDP,  $t_i^{\text{pre}} < t_i^{\text{post}}$  leads to potentiation (LTP) and, conversely,  $t_i^{\text{pre}} > t_i^{\text{post}}$  to depression (LTD). Thus,



$W(w; t_i^{\text{pre}} - t^{\text{post}})$  can be expressed as

$$\begin{aligned} f_+(w_i) \exp\left(\frac{t_i^{\text{pre}} - t^{\text{post}}}{\tau_+}\right) & \text{ if } t_i^{\text{pre}} < t^{\text{post}}, \\ -f_-(w_i) \exp\left(\frac{t_i^{\text{pre}} - t^{\text{post}}}{\tau_+}\right) & \text{ if } t_i^{\text{pre}} > t^{\text{post}}. \end{aligned} \quad (22)$$

Here decaying exponentials are used for illustration purpose.

We compare several schemes for the weight dependence that is defined by the scaling function  $f_{\pm}$ :

- Our recently proposed ‘log-STDP’ model [16] has a sublinear LTD (log-like saturating profile for  $f_-$ ) can produce to long-tail (lognormal-like) distributions of synaptic weights. Here we use

$$\begin{aligned} f_+(w) &= A_+ \exp(-w/w_0 \beta); \\ f_-(w) &= A_- \frac{\ln(1 + \alpha w/w_0)}{\ln(1 + \alpha)}, \end{aligned} \quad (23)$$

where  $w_0$  is a reference weight,  $\alpha$  controls the saturation degree of LTD and  $\beta$  the (slow) decay of LTP when the weight  $w$  increases.

- The ‘mlta-STDP’ model proposed by Gütig et al. [13] corresponds to:

$$\begin{aligned} f_+(w_i) &= A_+ (1 - w_i/w_{\max})^\gamma, \\ f_-(w_i) &= A_- (w_i/w_{\max})^\gamma, \end{aligned} \quad (24)$$

where  $\gamma$  scales from additive STDP with  $\gamma=0$  [6,12] to multiplicative STDP with  $\gamma=1$  that has a linear dependence for both LTP and LTD [39]. The “soft” bound  $w_{\max}$  is enforced on the weights. In numerical simulation, we will use  $\gamma \leq 0.1$  to obtain sufficiently strong competition between the synaptic weights.

- The special case of (24) with  $\gamma=0$  is weight independent, namely, additive STDP with  $f_{\pm}(w_i) = A_{\pm}$ , will be referred to as add-STDP.
- The ‘mlt-STDP’ model proposed by van Rossum et al. [13] corresponds to:

$$\begin{aligned} f_+(w_i) &= A_+, \\ f_-(w_i) &= A_- w_i. \end{aligned} \quad (25)$$

Baseline parameters used in numerical simulations are recapitulated in Table 1.

### Capturing the weight dynamics

The analysis is constrained to a single neuron excited by external inputs indexed by  $1 \leq i \leq N$ . The spike trains of the neuron and external input  $i$  are denoted by  $S_{\text{out}}(t)$  and  $S_i(t)$ , respectively. We use a previously developed framework [6,36] to analyze the effect of weight-dependent STDP on the input plastic weights  $w_i(t)$ .

The tractability of the present analysis relies on the condition that both the firing rates  $v_i$  and covariances  $C_{ij}$  are quasi-invariant

with respect to time  $t$  (but not for the time lag  $\tau$ ). We assume that learning occurs sufficiently slowly compared to the other neuronal mechanisms (i.e., PSP time constants and delays) and that the noise  $\zeta$  is not too strong, such that the drift (or first stochastic moment) of the weight dynamics essentially determines the emerging structure [14,77]. Under this “adiabatic” assumption, the weight evolution can be described by

$$\begin{aligned} \dot{w}_i(t) &\simeq \eta [Y[w_i; v_i(t); v_{\text{out}}(t)] + F_i^W(w_i; t)], \\ Y(w_i; v_i(t); v_{\text{out}}(t)) &= \begin{cases} (w_i) v_i(t) v_{\text{out}}(t) & \text{for STDP,} \\ a^{\text{in}} v_i(t) + a^{\text{out}} v_{\text{out}}(t) + (w_i) v_i(t) v_{\text{out}}(t) & \text{for STDP + SCC.} \end{cases} \end{aligned} \quad (26)$$

The weight update in (26) is the summation of two additive contributions. First, the rate-based contributions embodied by  $Y$  involve the time-averaged firing rates  $v_i$  and  $v_{\text{out}}$  for input  $i$  and the neuron, respectively, cf. (35). For weight-dependent STDP, it involves the integral value of the learning window (as a function of the current weight)

$$\tilde{w}(w_i) := \int W(w_i; \tau) d\tau. \quad (27)$$

Second, the covariance coefficient  $F_i^W$  incorporates the effect of the STDP on the time-averaged spike-time covariance  $F_i$  between the neuron and input  $i$ :

$$\begin{aligned} F_i^W(w_i; t) &:= \int_{-\infty}^{+\infty} W(w_i; \tau + d_i^{\text{ax}} - d_i^{\text{den}}) F_i(t, \tau) d\tau, \\ F_i(t, \tau) &:= \frac{1}{T} \int_{t-T}^t \langle S_{\text{out}}(t') S_i(t' + \tau) \rangle dt' - \\ &\quad \frac{1}{T} \int_{t-T}^t \langle S_{\text{out}}(t') \rangle dt' \frac{1}{T} \int_{t-T}^t \langle S_i(t'' + \tau) \rangle dt''. \end{aligned} \quad (28)$$

Note that the noise  $\zeta$  does not play a role in the weight drift evaluated here. In the Results section, we will show that the predicted weight specialization is valid even for a medium level of noise in STDP. In order to analyze the learning equation (26), we need to evaluate the neuronal firing rate  $v$  and covariance coefficients  $F_i$  in terms of the input parameters. For this purpose we need to specify the neuronal firing mechanism.

### Poisson neuron model

In the Poisson neuron model [6,13,14,19,36], the neuronal spiking mechanism is approximated by an inhomogeneous Poisson process driven by an intensity function  $\rho_{\text{out}}(t)$  in order to generate an output spike-time series  $S_{\text{out}}(t)$ . A presynaptic spike from input  $i$  induces a variation of  $\rho_{\text{out}}(t)$  referred to as the postsynaptic potential (PSP), which is determined by the synaptic weight  $w_i$ , the kernel function  $\epsilon_i$ , and the sum of the axonal and dendritic delays  $d_i^{\text{ax}} + d_i^{\text{den}}$ . We require  $\int \epsilon_i(t) dt = 1$  and, in order to preserve causality,  $\epsilon_i(t) = 0$  for  $t < 0$ . For illustration purposes, we choose a double exponential function for all  $\epsilon_i$ :

$$\epsilon_i(t) = \begin{cases} \frac{\exp(-t/\tau_A) - \exp(-t/\tau_B)}{\tau_A - \tau_B} & \text{for } t \geq 0, \\ 0 & \text{otherwise,} \end{cases} \quad (29)$$

with rise and decay time constants  $\tau_A < \tau_B$ , respectively. The “soma potential”  $\rho_{\text{out}}(t)$  sums the PSPs for all input spike times  $t_i^n$

$$\rho_{\text{out}}(t) = \sum_{i,n} w_i(t) \epsilon_i(t - t_i^n - d_i^{\text{ax}} - d_i^{\text{den}}). \quad (30)$$

Following (30), we obtain the consistency matrix equations for the firing rates and spike-time correlations:

$$\mathbf{v}_{\text{out}}(t) = \mathbf{w}(t) \mathbf{v}_{\text{in}}, \quad (31a)$$

$$\mathbf{F}^W(t) = \mathbf{w}(t) \mathbb{C}^Z[\mathbf{w}(t)]. \quad (31b)$$

Here  $\mathbf{w}$  and  $\mathbf{F}$  are  $N$ -row vectors and  $\mathbf{v}_{\text{in}}$  a  $N$ -column vector, whose elements are  $w_i$ ,  $F_i$  and  $v_i$ , respectively; bold capitals will be used for row vectors and bold lower-case characters for column vectors. The  $N \times N$  matrices  $\mathbb{C}^Z$  have elements that correspond to pairs of inputs  $(i, j)$ :

$$C_{ij}^Z(\mathbf{w}; t) = \int_{-\infty}^{+\infty} \chi_i(w_j; \tau) C_{ij}(t, \tau) d\tau \quad (32)$$

is reproduced in (3). Note the respective roles of indices  $i$  and  $j$ . The input covariance  $C_{ij}(\cdot, \tau)$  is assumed to be quasi-independent of time  $t$ , so  $\mathbf{F}^W(t)$  in (32) only depends on  $t$  through the weights  $w_j(t)$ , which slowly evolve due to STDP. The kernel functions  $\chi_i$  in (33) describe the interplay between STDP and the postsynaptic response kernels  $\epsilon_i$  that affects the weight dynamics:

$$\begin{aligned} \chi_i(w_j; \tau) &= \int W(w_j; \tau - r + d_i^{\text{ax}} - d_i^{\text{den}}) \epsilon_i(r + d_i^{\text{ax}} + d_i^{\text{den}}) dr \\ &= [W(w_j; \cdot) * \epsilon_i(\cdot)](\tau - 2d_i^{\text{den}}). \end{aligned} \quad (33)$$

The convolution indicated by  $*$  concerns the variable  $\tau$ . This equation is reproduced in Results, cf. (4). This means that the postsynaptic response crucially determines the effect of synaptic plasticity [19,27]. In particular, the dendritic delay  $d_i^{\text{den}}$  plays a distinct role compared to the axonal delay  $d_i^{\text{ax}}$  in that it shifts the kernel  $\chi_i$  as a function of  $\tau$  to the right, namely implying more potentiation for  $\tau=0$ . Because of the weight dependence, the kernel is modified via the scaling of both potentiation and depression for  $W(w_j; \cdot)$  when the strength  $w_j$  evolves, as illustrated in Fig. 2C. The combination of (26) and (31) leads to (2), where the dependence over time  $t$  is omitted.

### Description of input spiking structure

The following expressions allow us to deal with general inputs while at the same time satisfying the requirement for mathematical tractability. We denote by  $S_i(t)$  the spike train (Dirac comb) of input  $i$ . The corresponding time-averaged firing rate is defined as

$$v_i(t) := \frac{1}{T} \int_{t-T}^t \langle S_i(t') \rangle dt', \quad (34)$$

and, for a pair of inputs  $i$  and  $j$ , the spike-time cross-covariance  $C_{ij}$  is given by

$$\begin{aligned} C_{ij}(t, \tau) &:= \frac{1}{T} \int_{t-T}^t \langle S_i(t') S_j(t' + \tau) \rangle dt' - \\ &\quad \frac{1}{T} \int_{t-T}^t \langle S_i(t') \rangle dt' \frac{1}{T} \int_{t-T}^t \langle S_j(t'' + \tau) \rangle dt''. \end{aligned} \quad (35)$$

A double averaging is used in the above definitions:

- an ensemble average over the randomness (because the input spike trains will be generated using stochastic processes) denoted by the angular brackets  $\langle \dots \rangle$  and
- a smoothing over a period of duration  $T$ , chosen to be larger than the timescale of neuronal mechanisms, but smaller than the learning rate of STDP.

The separation of timescales implies that only correlations convey fast spiking information, whereas firing rates imply low-pass filtering. The covariance  $C_{ij}$  in (36) slightly differs from our previous framework [15,36]. It is actually the sum of two contributions: the stochastic covariance between the spike trains averaged over  $T$ , which relates to ‘spike coordination’:

$$\frac{1}{T} \int_{t-T}^t [\langle S_i(t') S_j(t' + \tau) \rangle - \langle S_i(t') \rangle \langle S_j(t' + \tau) \rangle] dt' \quad (36)$$

and the temporal covariance of the underlying rate functions, which we refer to as ‘rate covariation’:

$$\begin{aligned} &\frac{1}{T} \int_{t-T}^t \langle S_i(t') \rangle \langle S_j(t' + \tau) \rangle dt' - \\ &\frac{1}{T} \int_{t-T}^t \langle S_i(t') \rangle dt' \frac{1}{T} \int_{t-T}^t \langle S_j(t'' + \tau) \rangle dt''. \end{aligned} \quad (37)$$

For inputs generated using doubly stochastic processes [25], a double ensemble average has been used in a similar fashion to the combination of ensemble average and temporal integration here. With our convention, the graphical interpretation of correlogram  $C_{ij}(\cdot, \tau)$  is that peaks for positive values of  $\tau$  (right side) indicate that input  $i$  tends to fire earlier than  $j$ . For oscillatory inputs, if the closest peak to  $\tau=0$  is on the right side,  $i$  is phase-advanced compared to  $j$ .

### Conditions ensuring the existence of a stable fixed point for weight-dependent STDP

Here we examine the conditions under which there exists at least one fixed point such that (2) for plain STDP vanishes for all coordinates  $i$ , namely

$$\dot{w}_i = \eta [\tilde{w}(w_i) v_i (\sum_j w_j v_j) + \sum_j w_j \int_{-\infty}^{+\infty} W(w_i; \tau) C_{ji}^{\epsilon}(\tau) d\tau], \quad (38)$$

where  $C_{ji}^{\epsilon}$  denotes the convolution of the correlation with the PSP kernels  $\epsilon_j$ , reorganizing (33). We make a couple of assumptions here:

- The weight dependence is such that the LTD side of  $W(w; \tau)$  vanishes when  $w \rightarrow 0$ , whereas the LTP side vanishes for  $w \rightarrow +\infty$ . In particular, this implies that  $\tilde{w}(w)$  in (27) is a decreasing function of  $w$  and has a zero  $w_0 > 0$  where LTD balances LTP. This property is satisfied by both log-STDP and nlta-STDP.

- The inputs have positive correlations, meaning that  $C_{ij}^c(\tau) \geq 0$  for all pairs  $i$  and  $j$ .

We define for sake of simpler notation the following functions such that (39) reads  $\dot{w}_i(t) \propto \kappa(w_i, \{w_j\}) + \sum_{j \neq i} \psi_j(w_i, \{w_j\})$  with

$$\begin{aligned} \kappa(w_i, \{w_j\}) &:= (w_i)w_i \left( \sum_j w_j v_j \right) + w_i \int_{-\infty}^{+\infty} W(w_i; \tau) C_{ii}^c(\tau) d\tau \\ \psi_j(w_i, \{w_j\}) &:= w_j \int_{-\infty}^{+\infty} W(w_i; \tau) C_{ji}^c(\tau) d\tau, \end{aligned} \quad (39)$$

where  $\{w_j\}$  denotes the whole set of weights.

For each given  $i$ , the sign of the first term in  $\kappa(w_i, \{w_j\})$  is given by  $(w_i)$  alone and does not depend on  $\{w_j\}$ :

$$\frac{w_i}{\tilde{w}(w_i)} \left| \begin{array}{cc} 0 & w_0 \\ \oplus & \searrow & 0 & \searrow & \ominus \\ & & & & \end{array} \right. \quad (40)$$

where the circled signs indicate positive and negative values. The second term is zero for  $w_i = 0$  and for a sufficiently large  $w_i$ , it becomes negative (or barely positive) with the assumptions that LTP vanishes and  $C_{ij}^c(\tau) \geq 0$ . For all  $j \neq i$ , the sign of  $\psi_j(w_i, \{w_j\})$  is given by  $\int_{-\infty}^{+\infty} W(w_i; \tau) C_{ji}^c(\tau) d\tau$  and  $w_j$  scales its modulus linearly:

$$\frac{w_j}{g_j(w_i, \{w_j\})} \left| \begin{array}{cc} 0 & \infty \\ 0 & \nearrow & \oplus \\ \text{or} & \searrow & \ominus \\ 0 & & \end{array} \right. \quad (41)$$

Taken together, we have for an arbitrary small  $\delta$

$$\begin{aligned} f(0, \{w_j\}) &> 0, \\ g_j(0, \{w_j\}) &\geq -\delta \quad \text{for all } j \neq i; \end{aligned} \quad (42)$$

and there exists a set of constants  $L_i$  such that

$$\left. \begin{aligned} f(w_i, \{w_j\}) &< 0, \\ g_j(w_i, \{w_j\}) &\leq \delta \end{aligned} \right\} \quad \text{for } w_i \geq L_i. \quad (43)$$

These are sufficient conditions to prove that the expressions in (39) taken for all  $i$  have at least a global fixed point.

We first examine the illustrative case of  $N = 2$  weights. For any fixed  $w_2$ , the expression of  $\dot{w}_1$  in (39) satisfies the two properties of being positive on the axis  $w_1 = 0$  and becomes negative for large  $w_1$ , following (43) and (44). Consequently, for all  $w_2$ , there is at least one zero of  $\dot{w}_1$  as a function of  $w_1$ , and this zero is strictly positive and smaller than the upper bounds  $L_i$ . Moreover, the expression in (39) for  $i = 1$  is continuous with respect to both  $w_1$  and  $w_2$ , so the zeros form a continuous curve. Reciprocally, by inverting the indices, there is a similar zero for  $\dot{w}_2$ . Because of continuity, there is at least one intersection point for the sets of the zeros as in Fig. 4A, which nullifies  $\dot{w}_i$  for  $i = 1$  and 2.

In the general case of  $N \geq 2$  weights, the same properties in (43) and (44) ensure that, for each given  $i$ , (39) is positive on the hyperplane  $\{w_i = 0\}$  and negative on  $\{w_i = L_i\}$ . It follows that there is at least one zero for each  $w_j$ ,  $j \neq i$ . Thus, the continuous surface that contains the zeros of (39) for a given  $i$  contains a manifold of dimension  $N - 1$ . In the  $N$ -dimensional hypercube  $0 \leq w_j \leq L_j$ , all such manifolds for  $1 \leq i \leq N$  have at least one intersection point, since the ‘‘constraint’’ for being on the  $i$ -th manifold only concerns  $w_i$ . On the non-empty intersection set, all

derivatives  $\dot{w}_i$  vanish, meaning it consists of the fixed point(s) for the weight dynamics.

The structure of these manifolds is actually simple and allows us to determined to the global stability of the fixed point(s). For each  $i$ , the corresponding manifold separates the hypercube  $0 \leq w_j \leq L_j$  into two subspaces. On the side containing  $\{w_i = 0\}$ , we have  $\dot{w}_i > 0$ , whereas on the other side  $\{w_i = L_i\}$ ,  $\dot{w}_i < 0$ . Each manifold is thus a global attractor for the coordinate  $w_i$ , which guarantees global stability of their intersection set. The arrows in Fig. 4 illustrate the derivatives of  $w_1$  and  $w_2$ , which drive  $\mathbf{w}$  to its fixed point there.

Now, for negative correlations, (43) or (44) may not hold anymore and the zero of (39) may become negative or even not exist for some values of  $w_j$ . There is then no guarantee of a realizable global fixed-point, as illustrated in Fig. 4B. The analysis in this case will not be pursued here.

A similar demonstration applies for STDP+SCC when  $Y(w_i; v_i; v_{\text{out}})$  is positive for  $w_i = 0$  and decreases with  $w_i$ . This is the case when  $\gamma > 0$ , for which LTP and LTD vanish at the upper and lower bounds enforced on the weights, respectively, in addition to  $a^{\text{in}} > 0$ . With the further condition  $a^{\text{out}} < 0$  that ensures a fixed-point for the mean weight, the equivalent to  $\kappa$  decreases when the output firing rate  $v_{\text{out}} = \sum_j w_j v_j$  increases. Putting it all together, the existence of a fixed point is ensured for output firing rate that are not too high (and positive correlations).

### Relationship between the final weight distribution and the initial weight splitting

In the early period of the weight evolution, we can approximate the weight vector as proportional to the dominant eigenvector(s). Firstly, we consider the case of a single dominant eigenvalue, namely  $\mathbf{w} \propto \mathbf{v}_1$ . The spike-based term of (2) can be rewritten

$$\mathbf{w} \mathbb{C}^\lambda(\mathbf{w}) \simeq \mathbf{w} \mathbb{C}^\lambda(\mathbf{w}^*) + \mathbf{w} [\mathbb{C}^\lambda(\mathbf{w}) - \mathbb{C}^\lambda(\mathbf{w}^*)]. \quad (44)$$

Decomposing  $\mathbf{w} = \mathbf{v}_1 \exp(\lambda_1 t) + \mathbf{v}_\perp$  for some initial factor  $\mathbf{v}_1 > 0$  and  $\|\mathbf{v}_\perp\| \ll \mathbf{v}_1 \exp(\lambda_1 t)$ , the first term of the rhs  $\mathbf{w} \mathbb{C}^\lambda(\mathbf{w}^*)$  is dominated by its component  $\mathbf{v}_1 \lambda_1 \exp(\lambda_1 t) \mathbf{v}_1$ . This follows because  $\lambda_1$  is the largest eigenvalue. Now we further assume that the weight dependence is ‘‘weak’’ with respect to  $w$ . By this, we require the second term of the rhs above to be dominated by the first term. Together, this means that the vector elements of  $\mathbf{w} \mathbb{C}^\lambda(\mathbf{w})$  are ordered as those of  $\mathbf{v}_1$ . The fixed point of the dynamics in (2) can be approximated by

$$Y(\mathbf{w}; v_{\text{in}}; v_{\text{out}}) + \mathbf{w} \mathbb{C}^\lambda(\mathbf{w}) \simeq 0. \quad (45)$$

We assumed earlier that the weight dependence is such that the  $i$ -th component of  $Y$  is a decreasing of  $w_i$ . The implicit relationship in (46) indicates that the fixed point of  $\mathbf{w}$  is given by the reciprocal function to  $-Y$  applied on  $\mathbf{w} \mathbb{C}^\lambda(\mathbf{w})$ , which has its vector elements sorted in the same order as  $\mathbf{v}_1$  as we just explained. In other words,  $\mathbf{v}_1$  is expected to reflect the final weight distribution under the mentioned assumptions for a single dominant eigenvalue.

In the case of two complex conjugate dominant eigenvectors, a large imaginary part for  $\lambda_1$  implies a strong rotation-like evolution even at the early stage:  $\mathbf{w} \simeq 2\Re\{\alpha_1(0)\mathbf{v}_1 \exp(\lambda_1 t)\}$ . In this case, the equilibrium weight distribution may significantly differ from the initial splitting in the direction of  $\mathbf{v}_1$ . As an illustrative example, we consider two weights  $\mathbf{w} = (w_1, w_2)$  with

$$\mathbb{C}^Z(\mathbf{w}^*) = \begin{pmatrix} a & b \\ c & a \end{pmatrix}. \quad (46)$$

This expression corresponds to the cases of time-lagged correlated inputs in Figs. 8 and 9. When  $a > 0$ ,  $b < 0$  and  $c > 0$ ,  $\mathbb{C}^Z$  has complex conjugate eigenvalues  $a \pm i\sqrt{-bc}$ . Larger absolute values for  $b$  and  $c$  imply large imaginary parts. The spike-based effects on  $\mathbf{w}$  give  $\dot{\mathbf{w}} \simeq (aw_1 + cw_2, bw_1 + aw_2)$ . Starting from the homogeneous condition  $w_1 = w_2$ , it follows from  $b < 0$  that  $w_1$  increases faster  $w_2$ . If  $w_1$  becomes so large that  $w_2 = bw_1 + w_2 < 0$ , STDP results in LTP for  $w_1$  and LTD for  $w_2$  at the end of the learning epoch. This means that, despite an initial growth in the case  $a + b > 0$  (which is predicted by the eigenvectors),  $w_2$  is eventually depressed. In the general case, we also expect that some weights may become depressed because others experience stronger LTP due to STDP. In any case, the most strongly potentiated weights at the initial splitting should eventually be the winners of the synaptic competition.

### Response to correlated inputs after learning

Here we examine the spike transmission after learning, which is used to quantify mutual information in Results. To fix ideas, we present simple calculations for a neuron excited by a correlated pool of  $N_1$  inputs with homogeneous weight  $w_1$  and correlation strength  $c_1$ . The firing probability during a given time interval of  $D$  ms consecutive to a spike from input  $i$ , similar to a peristimulus time histogram (PSTH), can be seen as a measure of spike-based information transmission. It amounts to  $\int_{t_0}^{t_0+D} \text{Pr}\{S_{\text{out}}(t) | S_i(t_0)\} dt'$ , which relates to the correlation term of  $F_i$ , namely  $\langle S_{\text{out}}(t) S_i(t + \tau) \rangle$ , evaluated for  $\tau \in [-D, 0]$  and rescaled by the spike rate of  $S_i$ . For an isolated spike at time  $t_0$ , i.e., outside a correlated event such as that related to a reference  $\mathcal{R}_1$  in (11), the above integral can be approximated by

$$\int_{t_0}^{t_0+D} [v_{\text{out}}^* + w_1 \epsilon_1(t' - t_0)] dt' \simeq Dv_{\text{out}}^* + w_1 \left[ \int_0^D \epsilon_1(t') dt' \right]. \quad (47)$$

Likewise, for a spike involved in a correlated event, the average increase of firing probability is scaled up by the mean number of coincidentally firing inputs:

$$\int_{t_0}^{t_0+D} [v_{\text{out}}^* + N_1 \sqrt{c_1} w_1 \epsilon_1(t' - t_0)] dt' \simeq Dv_{\text{out}}^* + N_1 \sqrt{c_1} w_1 \left[ \int_0^D \epsilon_1(t') dt' \right]. \quad (48)$$

When the neuron has many inputs and a non-zero background firing activity, the group effect dominates with  $N_1 \sqrt{c_1} \gg 1$ , so we can neglect the term in  $w_1$  in (48). The ratio between (49) and (48) then becomes

$$\frac{Dv_{\text{out}}^* + N_1 \sqrt{c_1} w_1 \left[ \int_0^D \epsilon_1(t') dt' \right]}{Dv_{\text{out}}^* + w_1 \left[ \int_0^D \epsilon_1(t') dt' \right]} \simeq 1 + N_1 \sqrt{c_1} w_1 \frac{\int_0^D \epsilon_1(t') dt'}{Dv_{\text{out}}^*}. \quad (49)$$

To maximize this ratio, the optimal  $D$  lies beneath the values for which most of the integral of  $\epsilon$  is covered. Larger values for  $D$  beyond the timescale of the PSP kernel (e.g., several hundreds of ms as used for rate-based coding) lead to a smaller gain. With our parameters, we choose  $D = 25$  ms such that  $\int_0^D \epsilon_1(t') dt' \simeq 1$ . The lower the equilibrium mean firing rate  $v_{\text{out}}^*$ , the stronger

this signal-to-noise ratio is. For the Poisson neuron,  $v_{\text{out}}^*$  is also the variance of the firing rate, which can also be thought as a source of noise for rate coding. Note that from (26) with plain STDP, the equilibrium weight  $w_1^*$  for a pool of  $N_1$  instantaneously correlated inputs with strength  $c_1$  satisfies  $\tilde{w}(w_1^*) + N_1 c_1 w_1^* \chi(w_1^*, 0) = 0$ , which gives a theoretical prediction of the expressions above.

### Supporting information

**Text S1.** This section focuses on the situation where the spectrum of  $\mathbb{C}^Z$  contains imaginary eigenvalues. For add-STDP, this can lead to an oscillatory-like behavior of the weights. In contrast, weight-dependent STDP stabilizes the weight distribution.

**Figure S1.** Example of quasi-periodic evolution for plastic weights modified by add-STDP.

**Text S2.** We show that spike coordination and rate covariation can induce correlations of similar strength. We consider a neuron stimulated by inputs that have a common periodic firing rate. We show how the weight evolution is determined by the frequency of the input rate, the postsynaptic response and the STDP learning window.

**Figure S2.** Example of weight evolution that depends on the frequency of oscillatory input firing rates. The postsynaptic neuron can be trained to represent only a certain frequency range, similar to a band-pass filter.

### Supporting Information

**Figure S1** Instability of the emerging weight distribution. (A) The postsynaptic neuron is stimulated by  $m = 10$  pools. Nine pools exhibit correlated activity such that their respective inputs tend to fire in sequence a common reference  $\mathcal{R}_1$ , namely after a time lag equal to  $\bar{g}_l^1 = (l-1) \times 10$  ms for pool  $1 \leq l \leq m-1$ ; cf. (11) in the main text. The tenth pool has no correlation (x). (B) Spectrum of the corresponding input covariance matrix  $\mathbb{C}^Z$ . Comparison of the weight evolution for (C) add-STDP+SCC and (D) nta-STDP+SCC with  $\gamma = 0.03$ . The other STDP parameters are the same for both models:  $A_+ = 3$ ;  $A_- = 2$ ;  $\tau_+ = 8.5$  and  $\tau_- = 17$  ms;  $\eta = 2 \times 10^5$ ;  $a^{\text{in}} = 0.4$ ;  $a^{\text{in}} = -0.05$ ;  $w_{\text{max}} = 0.013$ . (1) The weight traces are represented in light gray. The mean weights over each input pool are in darker gray, apart from three that are displayed in color (thicker line). (2) Normalized distribution of the mean weights over each pool at different time of the simulation (time is indicated in thousands of seconds on the y-axis; blue corresponds to the earliest). For C1, the blue curve for  $t = 12000$  s has been reproduced in dotted line to compare it with distributions at two later times.

(EPS)

**Figure S2** Competition between instantaneous correlations and oscillatory firing rate. (A) Schematic representation of a single neuron stimulated by pool  $\bar{1}$  with instantaneous correlations and pool  $\bar{2}$  with an oscillatory firing rate (frequency  $f$ ). Their respective cross-correlograms are represented in red and blue. (B) Plot of the correlogram  $C_{ij}(\tau)$  between two oscillatory inputs from pool  $\bar{2}$  (blue trace). The two spike trains were simulate for 1000 s and the time bin for the x-axis is 1 ms. The predicted curve (black dashed line) corresponds to (S2) in Text S2: a cosine function with frequency  $f = 20$  Hz and amplitude  $v_0^2/2$  with  $v_0 = 10$  sp/s. (C) Theoretical prediction of the mean input-neuron correlation coefficients  $\bar{C}^Z$  for each input pool. The blue solid curve corresponds to the oscillatory pool  $\bar{2}$  and varies with the frequency  $f$ , cf. (S3) in Text S2. The red dashed and dashed-dotted

horizontal lines represent the instantaneous correlation of  $\bar{I}$  for  $\bar{c}_1 = 0.05$  and  $0.025$ , respectively; cf. (13) in the main text. The input firing rate is  $v_0 = 10$  sp/s for both pools. (D) Plots of the difference between the mean weights after 500 s of simulated time. Purple circles and green crosses correspond to  $\bar{c}_1 = 0.05$  (dashed line in B) and  $0.025$  (dashed-dotted line in B), respectively. Positive values indicate that the oscillatory pool is the winner at the end of the learning epoch. (E) Effect of dendritic delays on the STDP effect. The solid line is the same as in the case with  $d^{\text{den}} = 0$ , whereas the dashed and dashed-dotted curves correspond to  $d^{\text{den}} = 1.5$  and  $d^{\text{den}} = 3$  ms, respectively.

(EPS)

**Text S1** This section focuses on the situation where the spectrum of  $\mathbb{C}^{\mathcal{L}}$  contains imaginary eigenvalues. For add-STDP, this can lead to an oscillatory-like behavior of the weights. In contrast, weight-dependent STDP stabilizes the weight distribution.

(PDF)

## References

- Caporale N, Dan Y (2008) Spike timing-dependent plasticity: A Hebbian learning rule. *Annu Rev Neurosci* 31: 25–46.
- Larsen R, Rao D, Manis PB, Philpot BD (2010) STDP in the developing sensory neocortex. *Front Syn Neurosci* 2: 9.
- Gerstner W, Kempter R, van Hemmen JL, Wagner H (1996) A neuronal learning rule for submillisecond temporal coding. *Nature* 383: 76–78.
- Izhikevich EM, Desai NS (2003) Relating STDP to BCM. *Neural Comput* 15: 1511–1523.
- Burkitt AN, Meffin H, Grayden DB (2004) Spike-timing-dependent plasticity: The relationship to rate-based learning for models with weight dynamics determined by a stable fixed point. *Neural Comput* 16: 885–940.
- Kempter R, Gerstner W, van Hemmen JL (1999) Hebbian learning and spiking neurons. *Phys Rev E* 59: 4498–4514.
- Clopath C, Büsing L, Vasilaki E, Gerstner W (2010) Connectivity reflects coding: a model of voltage-based STDP with homeostasis. *Nat Neurosci* 13: 344–352.
- Masquelier T, Guyonneau R, Thorpe SJ (2008) Spike timing dependent plasticity finds the start of repeating patterns in continuous spike trains. *PLoS One* 3: e1377.
- Gilson M, Masquelier T, Hugues E (2011) STDP allows fast rate-modulated coding with Poisson spike trains. *PLoS Comput Biol* 7: e1002231.
- Scarpetta S, Zhaoping L, Hertz J (2002) Hebbian imprinting and retrieval in oscillatory neural networks. *Neural Comput* 14: 2371–2396.
- Lengyel M, Kwag J, Paulsen O, Dayan P (2005) Matching storage and recall: hippocampal spike timing-dependent plasticity and phase response curves. *Nat Neurosci* 8: 1677–1683.
- Song S, Miller KD, Abbott LF (2000) Competitive Hebbian learning through spike-timing-dependent synaptic plasticity. *Nat Neurosci* 3: 919–926.
- Gütig R, Aharonov R, Rotter S, Sompolinsky H (2003) Learning input correlations through nonlinear temporally asymmetric Hebbian plasticity. *J Neurosci* 23: 3697–3714.
- Meffin H, Besson J, Burkitt AN, Grayden DB (2006) Learning the structure of correlated synaptic subgroups using stable and competitive spike-timing-dependent plasticity. *Phys Rev E* 73: 041911.
- Gilson M, Burkitt AN, Grayden DB, Thomas DA, van Hemmen JL (2010) Representation of input structure in synaptic weights by spike-timing-dependent plasticity. *Phys Rev E* 82: 021912.
- Gilson M, Fukai T (2011) Stability versus neuronal specialization for STDP: Long-tail weight distributions solve the dilemma. *PLoS ONE* 6: e25339.
- Song S, Abbott LF (2001) Cortical development and remapping through spike timing-dependent plasticity. *Neuron* 32: 339–350.
- Cateau H, Kitano K, Fukai T (2008) Interplay between a phase response curve and spike-timing-dependent plasticity leading to wireless clustering. *Phys Rev E* 77: 051909.
- Gilson M, Burkitt AN, Grayden DB, Thomas DA, van Hemmen JL (2010) Emergence of network structure due to spike-timing-dependent plasticity in recurrent neuronal networks V: Selforganization schemes and weight dependence. *Biol Cybern* 103: 365–386.
- Izhikevich EM (2006) Proliferation: Computation with spikes. *Neural Comput* 18: 245–282.
- Lubenov EV, Siapas AG (2008) Decoupling through synchrony in neuronal circuits with propagation delays. *Neuron* 58: 118–131.
- Morrison A, Diesmann M, Gerstner W (2008) Phenomenological models of synaptic plasticity based on spike timing. *Biol Cybern* 98: 459–478.
- Gilson M, Burkitt AN, van Hemmen JL (2010) STDP in recurrent neuronal networks. *Front Comput Neurosci* 4: 23.
- van Rossum MCW, Turrigiano GG (2001) Correlation based learning from spike timing dependent plasticity. *Neurocomputing* 38: 409–415.
- Gerstner W, Kistler WM (2002) *Spiking neuron models: single neurons, populations, plasticity*. Cambridge University Press: 494 pp.
- Oja E (1982) A simplified neuron model as a principal component analyzer. *J Math Biol* 15: 267–273.
- Sprekeler H, Michaelis C, Wiskott L (2007) Slowness: An objective for spike-timing-dependent plasticity? *PLoS Comput Biol* 3: 1136–1148.
- Sejnowski TJ (1977) Storing covariance with nonlinearly interacting neurons. *J Math Biol* 4: 303–321.
- Savin C, Joshi P, Triesch J (2010) Independent component analysis with spiking neurons. *PLoS Comput Biol* 6: e1000757.
- Toyozumi T, Pfister JP, Aihara K, Gerstner W (2007) Optimality model of unsupervised spike-timing-dependent plasticity: Synaptic memory and weight distribution. *Neural Comput* 19: 639–671.
- Hennequin G, Gerstner W, Pfister J-P (2010) STDP in adaptive neurons gives close-to-optimal information transmission. *Front Comput Neurosci* 4: 143.
- Chechik G (2003) Spike-timing-dependent plasticity and relevant information maximization. *Neural Comput* 15: 1481–1510.
- Comon P (1994) Independent component analysis, a new concept? *Signal Process* 36: 287–314.
- Graupner M, Brunel N (2007) STDP in a bistable synapse model based on CaMKII and associated signaling pathways. *PLoS Comput Biol* 3: 2299–2323.
- Kempter R, Gerstner W, van Hemmen JL (2001) Intrinsic stabilization of output rates by spike-based Hebbian learning. *Neural Comput* 13: 2709–2741.
- Gilson M, Burkitt AN, Grayden DB, Thomas DA, van Hemmen JL (2009) Emergence of network structure due to spike-timing-dependent plasticity in recurrent neuronal networks I: Input selectivity - strengthening correlated input pathways. *Biol Cybern* 101: 81–102.
- Bi GQ, Poo MM (1998) Synaptic modifications in cultured hippocampal cells: Dependence on spike timing, synaptic strength, and postsynaptic cell type. *J Neurosci* 18: 10464–10472.
- van Rossum MCW, Bi GQ, Turrigiano GG (2000) Stable Hebbian learning from spike timing-dependent plasticity. *J Neurosci* 20: 8812–8821.
- Rubin J, Lee DD, Sompolinsky H (2001) Equilibrium properties of temporally asymmetric Hebbian plasticity. *Phys Rev Lett* 86: 364–367.
- Pfister JP, Gerstner W (2006) Triplets of spikes in a model of spike timing-dependent plasticity. *J Neurosci* 26: 9673–9682.
- Appleby PA, Elliott T (2006) Stable competitive dynamics emerge from multispike interactions in a stochastic model of spike-timing-dependent plasticity. *Neural Comput* 18: 2414–2464.
- Morrison A, Aertsen A, Diesmann M (2007) Spike-timing-dependent plasticity in balanced random networks. *Neural Comput* 19: 1437–1467.
- Burkitt AN, Gilson M, van Hemmen JL (2007) Spike-timing-dependent plasticity for neurons with recurrent connections. *Biol Cybern* 96: 533–546.
- Serre D (2010) *Matrices: theory and applications* (Volume 216 of Graduate Texts in Mathematics). Springer: 202 p.
- Pfister JP, Tass P (2010) STDP in oscillatory recurrent networks: theoretical conditions for desynchronization and applications to deep brain stimulation. *Front Comput Neurosci* 4: 22.
- Krumin M, Shoham S (2009) Generation of spike trains with controlled auto- and cross-correlation functions. *Neural Comput* 21: 1642–1664.
- Macke JH, Berens P, Ecker AS, Tolias AS, Bethge M (2009) Generating spike trains with specified correlation coefficients. *Neural Comput* 21: 397–423.
- Brette R (2009) Generation of correlated spike trains. *Neural Comput* 21: 188–215.

49. Bienenstock EL, Cooper LN, Munro PW (1982) Theory for the development of neuron selectivity - orientation specificity and binocular interaction in visual cortex. *J Neurosci* 2: 32–48.
50. Nowotny T, Rabinovich MI, Abarbanel HDI (2003) Spatial representation of temporal information through spike-timing-dependent plasticity. *Phys Rev E* 68: 011908.
51. Guyonneau R, VanRullen R, Thorpe SJ (2004) Temporal codes and sparse representations: A key to understanding rapid processing in the visual system. *J Physiol (Paris)* 98: 487–497.
52. Henry F, Dauce E, Soula H (2007) Temporal pattern identification using spike-timing dependent plasticity. *Neurocomputing* 70: 2009–2016.
53. Gilson M, Bärck M, Burkitt AN, van Hemmen JL (2012) Frequency selectivity emerging from spike-timing-dependent plasticity. *Neural Comput*. In press.
54. Turrigiano GG (2008) The self-tuning neuron: Synaptic scaling of excitatory synapses. *Cell* 135: 422–435.
55. Miller KD, Mackay DJC (1994) The role of constraints in Hebbian learning. *Neural Comput* 6: 100–126.
56. Xu L, White M, Schuurmans D (2009) Optimal reverse prediction: A unified perspective on supervised, unsupervised and semi-supervised learning. In: *Proceedings of the 26<sup>th</sup> International Conference on Machine Learning*; 2009; Montreal, Canada. ICML-09. URL <http://www.cs.ualberta.ca/~dale/papers.html>.
57. Bell A, Sejnowski T (1995) An information maximization approach to blind separation and blind deconvolution. *Neural Comput* 7: 1129–1159.
58. Gjorgjieva J, Clopath C, Audet J, Pfister JP (2011) A triplet spike-timing-dependent plasticity model generalizes the BienenstockCooperMunro rule to higher-order spatiotemporal correlations. *Proc Natl Acad Sci U S A* 108: 19383–19388.
59. Gütig R, Sompolinsky H (2006) The tempotron: a neuron that learns spike timingbased decisions. *Nat Neurosci* 9: 420–428.
60. Sjöström PJ, Turrigiano GG, Nelson SB (2001) Rate, timing, and cooperativity jointly determine cortical synaptic plasticity. *Neuron* 32: 1149–1164.
61. Appleby PA, Elliott T (2007) Multispike interactions in a stochastic model of spike-timingdependent plasticity. *Neural Comput* 19: 1362–1399.
62. Zou Q, Destexhe A (2007) Kinetic models of spike-timing dependent plasticity and their functional consequences in detecting correlations. *Biol Cybern* 97: 81–97.
63. Moreno-Bote R, Renart A, Parga N (2008) Theory of input spike auto-and cross-correlations and their effect on the response of spiking neurons. *Neural Comput* 20: 1651–1705.
64. Iannella NL, Launey T, Tanaka S (2010) Spike timing-dependent plasticity as the origin of the formation of clustered synaptic efficacy engrams. *Front Comput Neurosci* 4: 21.
65. Bar Ilan L, Gidon A, Segev I (2011) Interregional synaptic competition in neurons with multiple STDP-inducing signals. *J Neurophysiol* 105: 989–998.
66. von der Malsburg C (1981) The correlation theory of brain function. In: Domany E, van Hemmen JL, Schulten K, editors, *Models of Neural Networks II. Temporal Aspects of Coding and Information Processing in Biological Systems*. Springer. pp. 95–119.
67. Foffani G, Morales-Botello ML, Aguilar J (2009) Spike timing, spike count, and temporal information for the discrimination of tactile stimuli in the rat ventrobasal complex. *J Neurosci* 29: 5964–5973.
68. Kumar A, Rotter S, Aertsen A (2010) Spiking activity propagation in neuronal networks: reconciling different perspectives on neural coding. *Nat Rev Neurosci* 11: 615–627.
69. Byrnes S, Burkitt AN, Grayden DB, Meffin H (2011) Learning a sparse code for temporal sequences using STDP and sequence compression. *Neural Comput* 23: 2567–2598.
70. Mehta MR, Lee AK, Wilson MA (2002) Role of experience and oscillations in transforming a rate code into a temporal code. *Nature* 417: 741–746.
71. Masquelier T, Hugues E, Deco G, Thorpe SJ (2009) Oscillations, phase-of-firing coding, and spike timing-dependent plasticity: An efficient learning scheme. *J Neurosci* 29: 13484–13493.
72. Kohonen T (1982) Self-organized formation of topologically correct feature maps. *Biol Cybern* 43: 59–69.
73. Paugam-Moisy H, Martinez R, Bengio S (2008) Delay learning and polychronization for reservoir computing. *Neurocomputing* 71: 1143–1158.
74. Carnell A (2009) An analysis of the use of Hebbian and anti-Hebbian spike time dependent plasticity learning functions within the context of recurrent spiking neural networks. *Neurocomputing* 72: 685–692.
75. Maass W, Natschläger T, Markram H (2002) Real-time computing without stable states: A new framework for neural computation based on perturbations. *Neural Comput* 14: 2531–2560.
76. Cessac B, Rostro H, Vasquez J, Viville T (2009) How gibbs distributions may naturally arise from synaptic adaptation mechanisms. a model-based argumentation. *J Stat Phys* 136: 565–602.
77. van Hemmen JL (2001) Theory of synaptic plasticity. In: Moss F, Gielen S, editors. *Handbook of Biological Physics (Vol. 4: Neuro-informatics and neural modelling)*. Amsterdam: Elsevier. pp. 771–823.